Monthly Notices
of the
ROYAL ASTRONOMICAL SOCIETY

Mon. Not. R. Astron. Soc. **411,** 2750–2769 (2011) doi:10.1111/j.1365-2966.2010.17882.x

Spinning dust emission: the effect of rotation around a non-principal axis

Kedron Silsbee,[1] Yacine Ali-Haïmoud[2⋆] and Christopher M. Hirata[2]

[1]*California Institute of Technology, MSC 865, Pasadena, CA 91126, USA*
[2]*California Institute of Technology, Mail Code 350-17, Pasadena, CA 91125, USA*

Accepted 2010 October 15. Received 2010 August 15; in original form 2010 March 29

ABSTRACT

We investigate the rotational emission from dust grains that rotate around non-principal axes. We argue that in many phases of the interstellar medium, the smallest grains, which dominate spinning dust emission, are likely to have their nutation state (orientation of principal axes relative to the angular momentum vector) randomized during each thermal spike. We recompute the excitation and damping rates associated with rotational emission from the grain permanent dipole, grain–plasma interactions, infrared photon emission and collisions. The resulting spinning dust spectra generally show a shift towards higher emissivities and peak frequencies relative to previous calculations.

Key words: radiation mechanisms: non-thermal – dust, extinction – radio continuum: ISM.

1 INTRODUCTION

One of the difficulties in measuring the anisotropies in the cosmic microwave background (CMB) is that the interstellar medium (ISM) also emits microwave radiation through several mechanisms. This 'foreground' radiation must be modelled and subtracted in order to measure the cosmological parameters accurately using the CMB. The standard theory of ISM microwave emission contains three major emission mechanisms (e.g. Tegmark et al. 2000; Bennett et al. 2003; Fraisse et al. 2009): synchrotron radiation from relativistic electrons spiralling in the Galactic magnetic field; free–free radiation from ionized gas and thermal emission from dust grains. These are typically traced by external templates: low-frequency radio maps for the synchrotron (Haslam et al. 1982), Hα for the free–free (Finkbeiner 2003) and far-infrared continuum for the dust (Finkbeiner, Davis & Schlegel 1999).

Kogut et al. (1996a,b) reported a spatial correlation between Galactic microwave emission at 31.5, 53 and 90 GHz and the thermal infrared continuum from dust. They interpreted the microwave emission as dust-correlated free–free radiation, on top of the Rayleigh–Jeans tail of thermal emission from dust. Their observations were confirmed by de Oliveira-Costa et al. (1997), who measured the microwave intensity of the Galaxy at 30 and 40 GHz. Leitch et al. (1997) claimed the presence of an 'anomalous' component of Galactic microwave emission, which they observed as a signal at 14.5 and 32 GHz strongly correlated with the diffuse 100 μm intensity. It was far too bright to be thermal dust and had a flat spectrum across these bands, and low-frequency radio and Hα observations predicted far too little synchrotron or free–free emission to explain the signal. Leitch et al. (1997) proposed that the signal originated from hot gas at $T \geq 10^6$ K, which could produce free–free radiation but little Hα; however Draine & Lazarian (1998a) showed that this gas would cool rapidly and that keeping it hot was energetically unfeasible. Several alternative explanations have been proposed. Spinning dust emission is due to the rotation of small dust grains with permanent electric dipole moments. The basic mechanism has been known for decades (Erickson 1957; Hoyle & Wickramasinghe 1970; Rouan et al. 1992; Ferrara & Dettmar 1994), and was suggested as an explanation for the anomalous emission by Draine & Lazarian (1998b) (hereafter DL98b). Magnetic dust emission is due to thermal fluctuations of the magnetic dipole moments of grains including ferromagnetic or ferrimagnetic materials (Draine & Lazarian 1999). Hard synchrotron radiation would be a new synchrotron component from young (recently accelerated) high-energy electrons, proposed to be strongly correlated with the far-infrared emission from dust due to their common association with recent star formation (Bennett et al. 2003). Both the spinning and magnetic dust hypotheses predict an emission spectrum that peaks in the microwave (the former due to the rotation rates of the smallest grains, and the latter due to the gyrofrequency in ferromagnetic materials). The hard synchrotron hypothesis is now disfavoured due to the low polarization of the anomalous component observed by the *Wilkinson Microwave Anisotropy Probe* (*WMAP*; Page et al. 2007), its strong morphological correlation with dust maps (Finkbeiner 2004; Davies et al. 2006) and evidence that the anomalous emission has a rising spectrum at low frequencies (<20 GHz; de Oliveira-Costa et al. 1999; Finkbeiner, Langston & Minter 2004; Watson et al. 2005).

A key test to distinguish the various models for anomalous emission is to construct predicted emission spectra and compare them to observations. DL98b computed spinning dust spectra for a variety of interstellar environments, accounting for the main processes that affect grain rotation: collisions, grain–plasma interactions, infrared emission and radiation–reaction torque on the grain electric dipole moment. Model spinning dust spectra have been used

⋆E-mail: yacine@tapir.caltech.edu

extensively to test (and in some cases disfavour or rule out) the spinning dust hypothesis for the anomalous emission seen in the diffuse high-Galactic latitude ISM (Bennett et al. 2003; Finkbeiner 2004; Dobler & Finkbeiner 2008; Gold et al. 2009), in the Galactic Plane (e.g. Finkbeiner et al. 2004) and in dense regions such as molecular clouds (MC) (Finkbeiner 2004; Watson et al. 2005; Casassus et al. 2006, 2008) and H II regions (Dickinson et al. 2007, 2009), supernova remnants (Scaife et al. 2007), planetary nebulae (Casassus et al. 2007) and an external galaxy (NGC 6946; Murphy et al. 2010). Dobler, Draine & Finkbeiner (2009) have even used the anomalous emission seen by *WMAP* in the warm ionized medium (WIM; traced by Hα) to test dust models; they observe a factor of $\sim$3 *lower* anomalous emission than predicted, which they tentatively interpret as due to depletion of the smallest dust grains (the polycyclic aromatic hydrocarbons, or PAHs) in the WIM.

Recently, the grain rotation problem has been revisited by two theoretical groups. Ali-Haïmoud et al. (2009, hereafter AHD09) constructed a more detailed model of grain rotation, following the angular velocities of grains using a Fokker–Planck equation and re-evaluating the rotational excitation and damping rates using updated grain properties and a more sophisticated model for the grain–plasma interactions. They also released a public code, SPDUST, to compute spinning dust spectra for any input physical conditions and grain properties. Ysard & Verstraete (2009) presented a quantum-mechanical treatment of several of these processes and computed the resulting emission spectra.

The existing theoretical treatments of spinning dust, however, still contain a number of simplifying assumptions. One of the major uncertainties is the grain size distribution and typical dipole moment, however this uncertainty can be turned into a virtue by using it to constrain dust models (e.g. Dobler et al. 2009). Additionally, there are uncertainties in the physics of grain rotation, such as the validity of the Fokker–Planck approximation or the assumed properties such as the evaporation temperature of departing adsorbed atoms. Some of these pieces of physics are not readily amenable to improvement by theoretical calculations, but others are.

The purpose of this paper is to revisit the assumption by DL98b and AHD09 that grains rotate around the axis of largest moment of inertia due to internal dissipation processes. We argue in particular that PAHs in the diffuse and high UV flux phases are likely to be in a random nutation state. This is not a trivial detail: a dust grain rotating around a non-principal axis emits at multiple frequencies, including frequencies well in excess of the instantaneous grain angular velocity. The fact that electric dipole emission depends on the second derivative of the dipole moment $\ddot{\boldsymbol{\mu}}$ rather than just $\boldsymbol{\mu}$ enhances the importance of these higher frequencies.[1] We show in Section 4.1 that for disc-like grains, at fixed angular momentum incorporating a random nutation state increases the spinning dust emissivity by roughly an order of magnitude. Of course, having a random nutation state also modifies the processes that change grain angular momenta. We investigate each of the major processes and find that the typical grain angular momentum is reduced, but still find a factor of 1.6 increase in the peak spinning dust emissivity j_ν and a factor of 1.3 increase in the peak frequency for WIM conditions.[2]

This paper is organized as follows. Section 2 reviews the key parameters of the grain models. Section 3 describes the expected rotational state of grains and the formalism used in this paper (and in the updated SpDust) for describing the grain angular momentum distribution. Section 4 considers the electric dipole emission from grains rotating in a random nutation state. Subsequent sections consider spin-up and spin-down processes for the grains, taking account of nutation: Section 5 considers grain–plasma interactions; Section 6 considers infrared photon emission and Section 7 considers collisions. Predicted spinning dust spectra are shown in Section 8, where we also explore the sensitivity to some of our assumptions. We conclude in Section 9.

The physical processes affecting grains in non-uniform rotation are very complex, and this paper contains some unavoidably long calculations. The reader interested primarily in the results may skip directly from the end of Section 4.1 to the beginning of Section 8.

We note that Hoang, Draine & Lazarian (2010) have recently completed a related analysis in which axisymmetric dust grains are followed through a two-dimensional space of angular velocities ($\omega_\parallel$, $\omega_\perp$). Our analyses agree on the basic conclusion that allowing grains to rotate around a non-principal axis results in an increase in the spinning dust emissivity and an increase in the peak frequency.

2 GRAIN PROPERTIES

The physical properties of dust grains treated in this paper are unmodified from the model of AHD09. We briefly summarize the key points here, but refer to AHD09 and the references therein for details.

2.1 Size, shape and charge

The grain sizes are described by their volume-equivalent radius a, defined by $V = \frac{4}{3}\pi a^3$. The fiducial size distribution is taken from Weingartner & Draine (2001b). We consider only the carbonaceous grains because they dominate the population of the smallest grains (typically we find that grains with radii $\gtrsim$12 Å make no significant contribution to the spinning dust emission).

As in DL98b, the large grains are taken to be spherical and the smallest grains are taken to be planar, as appropriate for PAHs, and assume the transition to take place at $a_2 = 6$ Å or $N_{\rm C} \approx 100$ carbon atoms. For simplicity we assume the population of planar grains to be disc-like (although real PAHs can have much more complicated geometries), with a disc radius $R = (\frac{4}{3}a^3 d^{-1})^{1/2} \approx 7$ Å $(a/5{\rm Å})^{3/2}$, where we used the interlayer separation in graphite, $d = 3.35$ Å, to determine the volume-equivalent radius. In AHD09, it was found that the treatment of the smallest grains as planar was of only minimal importance, resulting in $\sim$10–20 per cent changes in the emissivity j_ν near the peak of the spectrum. This conclusion was, however, based on the assumption of rotation around the axis of greatest moment of inertia (e.g. Purcell 1979), which we argue here is not appropriate. Indeed, we find a substantial (typically a factor of $\sim$2) increase in the spinning dust emissivity as a consequence of the disc-like geometry of the PAHs.

[1] Ysard & Verstraete (2009) allowed for an arbitrary nutation state, but imposed the assumption that the grain dipole moment be exactly parallel to the axis of greatest moment of inertia, which eliminates three of the four frequencies of emission from an axisymmetric grain. They also did not re-consider the collisional and plasma excitation and drag coefficients.

[2] For ease of comparison with previous results, our WIM conditions are those of DL98b: density $n_{\rm H} = 0.1\,{\rm cm}^{-3}$, gas temperature $T = 8000$ K, H ionization fraction $n({\rm H}^+)/n_{\rm H} = 0.99$ and radiation field normalization $\chi = 1$.

The grain charge distribution calculation is unmodified from AHD09; it is based on the treatment of charging by electron and ion collisions (Draine & Sutin 1987; Weingartner & Draine 2001a) and photoelectric charging (Weingartner & Draine 2001a) assuming a standard interstellar radiation field (Mezger, Mathis & Panagia 1982; Mathis, Mezger & Panagia 1983) re-scaled by an environment-dependent multiplicative factor χ.

2.2 Dipole moments

The grain permanent dipole moment is one of the most uncertain properties as it is not constrained by the UV/optical absorption or IR emission data typically used in dust modelling (Weingartner & Draine 2001b; Li & Draine 2001). Our fiducial model is similar to that of AHD09 in assuming a multivariate Gaussian distribution (appropriate for the random summation of many bonds with dipole moments) with a root-mean-square value taken from DL98b: the intrinsic dipole moment is taken to be $\langle\mu_{\rm i}^2\rangle^{1/2} = \beta\, N_{\rm at}^{1/2}$, where $N_{\rm at}$ is the number of atoms and β is a normalization factor. The fiducial value is 0.38 D; this is highly uncertain, although we note that it is reasonable for PAHs that lack exact symmetries, e.g. the N-circumcoronene cation sequence ($C_{53}H_{18}N^+$, a PAH that would have zero dipole moment were it not for the single substitution) has a calculated dipole moment corresponding to $\beta = 0.16$–1.1 D depending on the position of the substitution (Hudgins, Bauschlicher & Allamandola 2005).

For a non-spherical grain, it makes sense to consider the orientation of the permanent dipole moment relative to the axis of greatest moment of inertia; that is, we can consider both the in-plane dipole moment $\mu_{\rm ip}$ and the out-of-plane moment $\mu_{\rm op}$. An in-plane dipole moment in a PAH could be produced by, e.g., nitrogen substitution, as suggested to reproduce the location of the 6.2 μm band (Hudgins et al. 2005), or by incomplete hydrogenation (or superhydrogenation) of the peripheral carbon atoms (Le Page, Snow & Bierbaum 2003). An out-of-plane dipole moment, as assumed by Ysard & Verstraete (2009), requires breaking the mirror-plane symmetry of the PAH, e.g. via warping due to pentagonal rings as occurs in corannulene, $C_{20}H_{10}$.[3]

In the absence of a definitive rationale for choosing the dipole moment to be in-plane or out-of-plane, we take for our fiducial model the isotropic ratio $\langle\mu_{\rm op}^2\rangle{:}\langle\mu_{\rm ip}^2\rangle = 1:2$ (i.e. assign the same moment on all three axes). This choice is very uncertain; however we find that the resulting spectra are only weakly sensitive to it – e.g. for the fiducial WIM model, we find only a ∼12 per cent change in the characteristic emitted frequency and a ∼10 per cent change in the total emitted power between the extreme cases of a purely in-plane dipole moment and a purely out-of-plane moment.

3 ROTATION OF A DISC-LIKE GRAIN

Here, we review the formalism to describe the rotation of a general axisymmetric grain, and the physics that determines the nutation angle distribution.

[3] We note that searches for corannulene rotational lines in the Red Rectangle have returned null results (Pilleri et al. 2009), but this does not rule out larger warped PAHs.

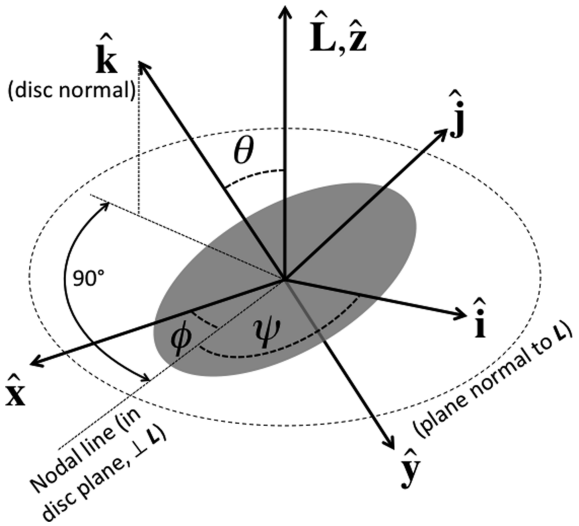

Figure 1. The definitions of the Euler angles used in this paper. The *xyz* axes correspond to the inertial frame and the *ijk* axes to the grain frame. The angular momentum vector lies in the $\hat{\boldsymbol{z}}$ direction, the normal to the grain disc lies in the $\hat{\boldsymbol{k}}$ direction and the grain permanent electric dipole moment lies in the *ik*-plane.

3.1 General description

We focus here on the case of an oblate axisymmetric dust grain, i.e. one with principal moments of inertia $I_1 = I_2 < I_3$. For a planar grain, which is a reasonable model for a PAH, one has $I_3 = 2I_1$.[4] In free solid-body rotation, the angular momentum $\boldsymbol{L}$ and rotational energy $E_{\rm rot}$ are conserved; this implies that the angle θ between the grain symmetry axis and the angular momentum vector is also conserved. We may choose the z-axis to be along the angular momentum vector, so that θ is one of the Euler angles of the grain (see Fig. 1). The remaining two Euler angles ϕ, ψ then advance at a rate (e.g. equations 8.46,47 of Hand & Finch 1998)

$$\dot{\phi} = \frac{L}{I_1} \tag{1}$$

and

$$\dot{\psi} = -L(I_1^{-1} - I_3^{-1})\cos\theta. \tag{2}$$

We note that $\dot{\psi}$ may have either sign, but one always has $|\dot{\psi}| < \dot{\phi}$.

The rotational energy is given by

$$E_{\rm rot} = \frac{L^2}{2I_1} - \frac{L^2}{2}(I_1^{-1} - I_3^{-1})\cos^2\theta. \tag{3}$$

The quantum-mechanical description of the system will occasionally be useful (e.g. for counting states) even though the calculation of this paper is in the classical regime, as DL98b showed that in general $L \gg \hbar$ even for the smallest grains.[5] This description is the same as that for a rotating oblate molecule (e.g. Kroto 1992, section 3.9): the good quantum numbers are the total angular momentum quantum number J, with total angular momentum $\hbar\sqrt{J(J+1)}$; its projection on the grain three-axis $\hbar K$ and its projection on the inertial frame z-axis $\hbar M$. These all take integer values, with $J \geq 0$ and

[4] For warped PAHs, I_3/I_1 is not exactly 2; but it is e.g. 1.93 for corannulene according to the structural parameters given in Hedberg et al. (2000).

[5] For the same reason, we neglect issues of nuclear spin statistics that can arise at small values of J and K for molecules with non-trivial symmetry groups.

$|K|, |M| \leq J$. In the case where the lab frame z-axis is aligned with the conserved angular momentum, we have $M = J$. The nutation angle θ satisfies

$$\cos\theta = \frac{K}{\sqrt{J(J+1)}} \approx \frac{K}{J} \quad \text{for } J \gg 1. \tag{4}$$

3.2 Rotational configuration

The rotational state of PAHs undergoing thermal spikes has been studied in many previous works, particularly those concerned with the polarization of the PAH emission bands (e.g. Leger 1988; Sironi & Draine 2009). Here, we recount the key results and explain why we expect PAHs in the diffuse ISM phases to generally *not* rotate around a principal axis of inertia.

3.2.1 Effect of thermal spikes on grain rotation

The rotational state of an oblate dust grain is generically described by both an angular momentum L and the angle θ between this angular momentum and the axis of symmetry of the grain. For large grains, we expect dissipation to bring the grain to the states of minimum rotational energy at fixed angular momentum, i.e. $\theta = 0$ or $\theta = \pi$. For the small grains that dominate spinning dust emission, however, the physics is different because the grain undergoes occasional thermal spikes (following absorption of each UV photon) followed by cooling into the vibrational ground state. During thermal spikes, rapid transfer of energy is expected to occur between rotational and vibrational degrees of freedom. This results in a probability distribution for θ:

$$P(\theta|L)d\theta \propto \exp\left[\frac{-E_{\rm rot}(L,\theta)}{kT_{\rm vib}}\right] g(\theta|L)d\theta, \tag{5}$$

where $g(\theta|L) \propto \sin\theta$ is the density of states.[6] This leads to a maximum entropy distribution $P(\theta|L) \propto \sin\theta$ in the limit of $kT_{\rm vib} \gg E_{\rm rot}$, which holds immediately after a UV photon absorption. As the grain cools, $T_{\rm vib}$ drops. However, as the grain cools, the density of vibrational states drops, and at some temperature $T_{\rm fr}$ the vibration–rotation energy transfer freezes out. We thus expect that the distribution of θ after a thermal spike freezes out at

$$P(\theta|L)d\theta \propto \exp\left[\frac{-E_{\rm rot}(L,\theta)}{kT_{\rm fr}}\right] g(\theta|L)d\theta. \tag{6}$$

We consider disc-like grains for $a \leq 6$ Å ($N_{\rm C} \leq 100$ carbon atoms). We note that using the Draine & Li (2001) model for the vibrational spectrum, the fundamental mode is expected to be at $h\nu_1/k = 70(N_{\rm C}/100)^{-1/2}$ K. The freeze-out temperature should be at least a few times greater than this, depending on the mode spectrum and strength of anharmonic and vibration–rotation couplings. This is greater than the rotational kinetic energy in most of the ISM phases [or similar to it for high radiation density environments such as photodissociation regions (PDRs)]. Thus, we expect that in most environments, $kT_{\rm fr}$ exceeds the rotational energy, and the direction of the grain symmetry axis is almost completely isotropized [$P(\theta|L) \propto \sin\theta$] following each thermal spike.

[6] An easy way to see that the density of states is $\propto \sin\theta$ is to note that at fixed total angular momentum J, since $K = \sqrt{J(J+1)}\cos\theta$, the number of states per unit $\cos\theta$ is constant, and hence the number of states per unit θ is $\propto \sin\theta$.

3.2.2 Frequency of thermal spikes

Given the major effect of thermal spikes on the rotational state, it is important to consider how the time between thermal spikes $\tau_{\rm abs}$ compares to the time-scale for changes in grain angular momentum $\tau_{\rm rot}$. The characteristic time-scale between UV photon absorptions for a grain of volume-equivalent radius a is

$$\tau_{\rm abs} = \left[\pi a^2 c \int Q_{\rm abs}(a;\nu)\frac{u_\nu}{h\nu}{\rm d}\nu\right]^{-1}, \tag{7}$$

where $u_\nu = \chi u_{\nu,\rm ISRF}$ is the ambient radiation field and $\pi\, a^2\, Q_{\rm abs}$ is the absorption cross-section.

The characteristic rotational damping (or excitation, in steady-state) time-scale for such a grain is $\tau_{\rm rot} \equiv L|\frac{{\rm d}L}{{\rm d}t}|^{-1}$, where L is the characteristic angular momentum of the grain and $\frac{{\rm d}L}{{\rm d}t}$ is the rotational damping rate evaluated at L. Evaluating $\tau_{\rm rot}$ requires an analysis of the rotational dynamics. The AHD09 analysis suggests

$$\tau_{\rm rot} \approx \min\left[\frac{\tau_{\rm H}}{F}, \left(\frac{\tau_{\rm H}\tau_{\rm ed}}{G}\right)^{1/2}\right], \tag{8}$$

where F and G are the normalized damping and excitation rates; and $\tau_{\rm H}$ and $\tau_{\rm ed}$ are the idealized characteristic damping time-scales through collisions with hydrogen atoms and electric dipole radiation, respectively (see AHD09 and the next section for their precise definitions, and note that $\tau_{\rm ed}$ is defined for thermally rotating grains, but that the actual dipole damping time varies depending on whether rotation is sub- or super-thermal).[7]

Since the smallest grains rotate fastest and determine the peak of the spinning dust spectrum, we evaluate the above time-scales at the smallest grain size $a = 3.5$ Å, for the idealized interstellar environments defined in DL98b (table 1). We show these time-scales in Table 1, for both the case of $\theta = 0$ (AHD09) and isotropized θ (using the formulae in this paper).

In the diffuse ISM phases [cold neutral medium (CNM), warm neutral medium (WNM), WIM], thermal spikes occur with a rate at least nearly four to six times higher than the processes that change the grain angular momentum. The rate difference is even more pronounced in regions of high radiation intensity [reflection nebula (RN), PDR], where the small grains can absorb several hundreds of photons during the time it takes to change their angular momentum. Therefore, we expect an isotropic distribution $P(\theta|L) \propto \sin\theta$ in these phases. Note that this is *not* true of regions of lower radiation density (DC, MC), where thermal spikes occur every few hundreds to thousands of years and $\tau_{\rm abs} \gg \tau_{\rm rot}$. In such cases, other processes will dominate the distribution of θ and the result may be in between complete isotropization (as assumed here) and perfect rotation around the I_3 axis ($\theta = 0$; assumed in DL98b and AHD09). An example of such an intermediate case would be the Maxwellian distribution for θ (Jones & Spitzer 1967; Lazarian & Roberge 1997).

3.3 Angular momentum distribution

The previous spinning dust analysis by AHD09 followed the Fokker–Planck equation for the probability distribution of grains

[7] In equation (8) the damping time is typically $\tau_{\rm H}/F$ when linear drag processes dominate. When electric dipole damping dominates, e.g. in the WIM, the angular velocity is typically $(G\tau_{\rm ed}/\tau_{\rm H})^{1/4}$ times the thermal angular velocity $\omega_{\rm th} = (kT/I_3)^{1/2}$ (AHD09). Since electric dipole emission torque scales as ω^3 instead of ω, the actual time-scale for electric dipole damping is then $\tau_{\rm ed}(\omega/\omega_{\rm th})^{-2}$, or $(\tau_{\rm H}\,\tau_{\rm ed}/G)^{1/2}$.

Table 1. Characteristic time-scales for UV photons absorption and rotational damping for idealized interstellar phases. The rotational damping time is shown for grains rotating about their axis of greatest inertia ('case 1', as assumed in DL98b, AHD09), and for grains which are randomly oriented with respect to their angular momentum ('case 2', the subject of the present work). All values are for the smallest grains ($a = 3.5$ Å or $N_{\rm C} = 20$).

Phase	DC	MC	CNM	WNM	WIM	RN	PDR
$\tau_{\rm abs}$ (s)	2.0×10^{11}	2.0×10^{9}	2.0×10^{7}	2.0×10^{7}	2.0×10^{7}	2.0×10^{4}	6.6×10^{3}
$\tau_{\rm rot}$ (s) [case 1]	1.6×10^{7}	9.5×10^{7}	1.9×10^{8}	2.8×10^{8}	2.1×10^{8}	7.0×10^{6}	1.4×10^{6}
$\tau_{\rm rot}$ (s) [case 2]	1.4×10^{7}	4.1×10^{7}	8.2×10^{7}	1.2×10^{8}	9.0×10^{7}	6.9×10^{6}	1.1×10^{6}

as a function of their angular velocity vector $\boldsymbol{\omega}$. Since $\boldsymbol{\omega}$ is not conserved for a non-spherical grain, the proper variable to follow instead is the angular momentum $\boldsymbol{L}$. However, in order to maintain a simple connection to previous work, we define the variable:

$$\boldsymbol{\Omega} \equiv \frac{\boldsymbol{L}}{I_3}. \tag{9}$$

This is the angular velocity that the grain would have *if* it were able to dissipate the energy associated with its nutation; we note that the magnitude of the actual angular velocity $\boldsymbol{\omega}$ satisfies $|\boldsymbol{\omega}| \geq |\boldsymbol{\Omega}|$. In this paper, the Fokker–Planck equation is constructed in terms of $\boldsymbol{\Omega}$.

For disc-like grains considered in this paper, with $I_1 = \frac{1}{2} I_3$, the rotational rates become

$$\dot{\phi} = 2\Omega \ \text{ and } \ \dot{\psi} = -\Omega \cos\theta. \tag{10}$$

These results will be needed repeatedly throughout the paper.

3.3.1 Form of the Fokker–Planck equation

Following the treatment of AHD09, we write the general Fokker–Planck equation for the equilibrium distribution of $\boldsymbol{\Omega}$:

$$\frac{\partial}{\partial \Omega^i}\left[D^i(\boldsymbol{\Omega}) f_a(\boldsymbol{\Omega})\right] + \frac{1}{2}\frac{\partial^2}{\partial \Omega^i \partial \Omega^j}\left[E^{ij}(\boldsymbol{\Omega}) f_a(\boldsymbol{\Omega})\right] = 0. \tag{11}$$

The Fokker–Planck coefficients are

$$D^i(\boldsymbol{\Omega}) \equiv -\lim_{\delta t \to 0} \frac{\langle \delta \Omega^i \rangle}{\delta t} \ \text{ and } \ E^{ij}(\boldsymbol{\Omega}) \equiv \lim_{\delta t \to 0} \frac{\langle \delta \Omega^i \delta \Omega^j \rangle}{\delta t}. \tag{12}$$

Here $\boldsymbol{D}$ denotes the mean drift in $\boldsymbol{\Omega}$, and $\mathbf{E}$ denotes the diffusion coefficient tensor.

It is important to note that, because of the isotropic distribution of the direction of the grain symmetry axis (see Section 3.2), these coefficients are averaged over the angle θ. More explicitly,

$$D^i(\boldsymbol{\Omega}) \equiv -\frac{1}{2}\int_0^{\pi} \lim_{\delta t \to 0} \frac{\langle \delta \Omega^i \rangle}{\delta t}(\boldsymbol{\Omega}, \theta) \sin\theta \, {\rm d}\theta \ , \tag{13}$$

and similarly for E^{ij} $(\boldsymbol{\Omega})$.

We now assume an isotropic medium, which is a good approximation so long as we are considering the total intensity spectrum (small deviations from isotropy would result in net polarization, which is not the subject of this paper). The drift and diffusion terms can then be decomposed as

$$\boldsymbol{D}(\boldsymbol{\Omega}) = D(\Omega)\hat{\boldsymbol{e}}_{\boldsymbol{\Omega}} \tag{14}$$

and

$$\mathbf{E}(\boldsymbol{\Omega}) = E_{\parallel}(\Omega)\hat{\boldsymbol{e}}_{\boldsymbol{\Omega}} \otimes \hat{\boldsymbol{e}}_{\boldsymbol{\Omega}} + E_{\perp}(\Omega)(\mathbf{1} - \hat{\boldsymbol{e}}_{\boldsymbol{\Omega}} \otimes \hat{\boldsymbol{e}}_{\boldsymbol{\Omega}}), \tag{15}$$

where $\hat{\boldsymbol{e}}_{\boldsymbol{\Omega}}$ is the unit vector in the direction of $\boldsymbol{\Omega}$ and $\mathbf{1}$ is the identity matrix. The function $D(\Omega)$ then denotes the rate of damping of rotation, while $E_{\parallel}(\Omega)$ and $E_{\perp}(\Omega)$ measure random excitation of the magnitude and direction of the angular momentum vector. AHD09 then show that the overall distribution function for Ω satisfies the equation

$$\frac{{\rm d}f_a(\Omega)}{{\rm d}\Omega} + 2\frac{\tilde{D}(\Omega)}{E_{\parallel}(\Omega)} f_a(\Omega) = 0, \tag{16}$$

where

$$\tilde{D}(\Omega) \equiv D(\Omega) + \frac{E_{\parallel}(\Omega) - E_{\perp}(\Omega)}{\Omega} + \frac{1}{2}\frac{{\rm d}E_{\parallel}(\Omega)}{{\rm d}\Omega}. \tag{17}$$

Note that $\tilde{D}$ is simply equal to D if the excitation rates are isotropic and independent of Ω. This is true for some of the mechanisms described, but plasma excitation in particular has non-trivial Ω dependence and here equation (17) is necessary.

3.3.2 Excitation and damping coefficients

The $\tilde{D}(\Omega)$ and $E_{\parallel}(\Omega)$ are sufficient to write the Fokker–Planck equation but are non-trivial to interpret and vary wildly as a function of grain size. For this reason, DL98b introduced dimensionless coefficients F and G that describe damping and excitation rates relative to those that one would obtain from the ballistic impact of hydrogen atoms on an idealized spherical grain. These are, for process X,

$$F_X(\Omega) \equiv \frac{\tau_{\rm H}}{\Omega}\tilde{D}_X(\Omega) \tag{18}$$

and

$$G_X(\Omega) \equiv \frac{I_3 \tau_{\rm H}}{2kT} E_{\parallel,X}(\Omega), \tag{19}$$

where $\tau_{\rm H}$ is the idealized damping time-scale (whose precise definition is given in AHD09) and T is the gas temperature.

3.3.3 Fluctuation–dissipation theorem

In their analysis of spherical grains, DL98b and AHD09 argued that processes resulting from interaction with a thermal bath at temperature T_X (notably plasma drag and excitation) should obey the fluctuation–dissipation theorem, $\tilde{D} = I_3 \Omega E_{\parallel}/2kT_X$. The equivalent result for excitation and damping coefficients is that $F = (T/T_X)G$. No such result can apply here because the randomization of the nutation degree of freedom during thermal spikes renders the notion of a 'thermal' distribution for Ω not internally consistent. However, the fluctuation–dissipation theorem's close cousin, the principle of detailed balance, can be of some use if one computes damping and excitation of the actions $|\boldsymbol{L}| \approx \hbar J$ and $L\cos\theta = \hbar K$ for individual (J, K) levels, and then averages the resulting coefficients over K. We will need to use this technique to compute the plasma drag on a grain rotating around a non-principal axis.

4 ELECTRIC DIPOLE EMISSION

Our task in computing the emission spectrum falls into two major steps. One is to relate the distribution of rotational states $f_a(\Omega)$ to the observable emission. The other, harder task, is to compute the Fokker–Planck coefficients arising from each mechanism. We consider the emission process in this section, and then proceed to consider the damping and excitation mechanisms in later sections.

For the case of a grain rotating around a principal axis of inertia, the grain merely rotates with constant angular velocity $\boldsymbol{\omega}$ and emits monochromatic radiation at frequency $\omega/(2\pi)$. Thus, in these models (DL98b, AHD09) the emitted spectrum from a particular grain is built up from its dipole moment and the probability distribution for ω. The non-uniform rotation case treated here is more complicated, as we will see that four frequencies are emitted.

4.1 Emission spectrum

Our first step in the analysis is to consider how the electric dipole moment $\boldsymbol{\mu}$ of a grain varies as a function of time. We define the $\hat{\boldsymbol{i}}$, $\hat{\boldsymbol{j}}$ and $\hat{\boldsymbol{k}}$ vectors to form a grain-fixed basis with $\hat{\boldsymbol{k}}$ along the symmetry axis. Without loss of generality, $\boldsymbol{\mu}$ may be assumed to be in the plane defined by $\hat{\boldsymbol{i}}$ and $\hat{\boldsymbol{k}}$. Then,

$$\boldsymbol{\mu} = \mu_{\rm ip}\hat{\boldsymbol{i}} + \mu_{\rm op}\hat{\boldsymbol{k}}, \tag{20}$$

where $\mu_{\rm ip}$ and $\mu_{\rm op}$ are the in-plane and out-of-plane components of the dipole moment, respectively.

We now consider the behaviour of the dipole moment relative to an inertial coordinate system. We choose the inertial $\hat{\boldsymbol{z}}$ axis to be parallel to the angular momentum; then we define the 3×3 orthogonal matrix $\mathbf{U}$ with elements $U_{xi} = \hat{\boldsymbol{x}} \cdot \hat{\boldsymbol{i}}$, and similarly for the other eight entries. The entries involving $\hat{\boldsymbol{i}}$ and $\hat{\boldsymbol{k}}$ are needed here:

$$\begin{aligned}
U_{xi} &= \cos\phi\cos\psi - \cos\theta\sin\psi\sin\phi,\\
U_{yi} &= \cos\psi\sin\phi + \cos\phi\cos\theta\sin\psi,\\
U_{zi} &= \sin\psi\sin\theta,\\
U_{xk} &= \sin\theta\sin\phi,\\
U_{yk} &= -\sin\theta\cos\phi \ \text{ and}\\
U_{zk} &= \cos\theta.
\end{aligned} \tag{21}$$

For our purposes, it is most convenient to express the first two of these using the product-to-sum rule:

$$\begin{aligned}
U_{xi} &= \frac{1}{2}[(1-\cos\theta)\cos(\psi-\phi)\\
&\quad + (1+\cos\theta)\cos(\psi+\phi)] \ \text{ and}\\
U_{yi} &= \frac{1}{2}[(1+\cos\theta)\sin(\psi+\phi)\\
&\quad + (1-\cos\theta)\sin(\phi-\psi)].
\end{aligned} \tag{22}$$

The advantage of this formulation is that since $\dot{\psi}$ and $\dot{\phi}$ are constant, we have expressed all required components of $\mathbf{U}$ as sinusoidal functions of time. Each sinusoidal function directly emits a δ-function spectrum at its frequency. One can see that the above components of $\mathbf{U}$ oscillate with the four (angular) frequencies $\dot{\phi}$, $|\dot{\psi}|$, $\dot{\phi}+\dot{\psi}$ and $\dot{\phi}-\dot{\psi}$. From equation (20) we see that the same frequencies are present in $\boldsymbol{\mu}$ (as observed in inertial coordinates).

The power emitted by an accelerating dipole is given by

$$P = \frac{2\ddot{\boldsymbol{\mu}}^2}{3c^3}. \tag{23}$$

From equations (20) and (22), we see we may write $\ddot{\boldsymbol{\mu}}$ as

$$\begin{aligned}
\ddot{\boldsymbol{\mu}} = &\Big\{-\frac{1}{2}\mu_{\rm ip}[(1-\cos\theta)(\ddot{\psi}-\ddot{\phi})^2\cos(\psi-\phi)\\
&+(1+\cos\theta)(\ddot{\psi}+\ddot{\phi})^2\cos(\psi+\phi)]\\
&-\mu_{\rm op}\ddot{\phi}^2\sin\theta\sin\phi\Big\}\hat{\boldsymbol{x}}\\
&+\Big\{-\frac{1}{2}\mu_{\rm ip}[(1+\cos\theta)(\ddot{\psi}+\ddot{\phi})^2\sin(\psi+\phi)\\
&+(1-\cos\theta)(\ddot{\phi}-\ddot{\psi})^2\sin(\phi-\psi)]\\
&+\mu_{\rm op}\ddot{\phi}^2\sin\theta\cos\phi\Big\}\hat{\boldsymbol{y}}\\
&-\mu_{\rm ip}\ddot{\psi}^2\sin\theta\sin\psi\,\hat{\boldsymbol{z}}.
\end{aligned} \tag{24}$$

We observe that when we average over many cycles of ϕ and ψ, all terms average to zero except those which can be expressed in terms of just $\sin^2\omega$ or $\cos^2\omega$, where ω is one of $\dot{\phi}$, $\dot{\psi}$, $\dot{\phi}-\dot{\psi}$ of $\dot{\phi}+\dot{\psi}$. Each of these terms contributes power which is emitted at frequency ω. We find the following.

(i) At frequency $\dot{\phi}+\dot{\psi}$, the emitted power is

$$P_{\dot{\phi}+\dot{\psi}} = \frac{\mu_{\rm ip}^2(\dot{\psi}+\dot{\phi})^4(1+\cos\theta)^2}{6c^3}. \tag{25}$$

(ii) At frequency $\dot{\phi}-\dot{\psi}$, the emitted power is

$$P_{\dot{\phi}-\dot{\psi}} = \frac{\mu_{\rm ip}^2(\dot{\phi}-\dot{\psi})^4(1-\cos\theta)^2}{6c^3}. \tag{26}$$

(iii) At frequency $\dot{\phi}$, the emitted power is

$$P_{\dot{\phi}} = \frac{2\mu_{\rm op}^2\dot{\phi}^4\sin^2\theta}{3c^3}. \tag{27}$$

(iv) At frequency $|\dot{\psi}|$, the emitted power is

$$P_{|\dot{\psi}|} = \frac{\mu_{\rm ip}^2\dot{\psi}^4\sin^2\theta}{3c^3}. \tag{28}$$

The overall emitted spectrum from a grain of given angular momentum L is then obtained by finding the amount of power emitted in a range of angular frequencies $(\omega, \omega+{\rm d}\omega)$ using both the emitted power for each of the four components and the probability of that component falling in the range $(\omega, \omega+{\rm d}\omega)$. Consider, for example, the $\dot{\phi}+\dot{\psi}$ component. Letting $\omega = \dot{\phi}+\dot{\psi}$, we can see that ω is bounded by

$$\frac{L}{I_3} \le \omega \le 2\frac{L}{I_1} - \frac{L}{I_3}, \quad \text{i.e.} \quad \Omega \le \omega \le 3\Omega. \tag{29}$$

Within this range, the probability distribution for ω can be found using

$$\omega = \dot{\phi}+\dot{\psi} = \frac{L}{I_1} - \left(\frac{L}{I_1} - \frac{L}{I_3}\right)\cos\theta = \Omega(2-\cos\theta). \tag{30}$$

Since $\cos\theta$ is uniformly distributed between -1 and 1 with density $\frac{1}{2}$, the probability density for ω is then

$${\rm Prob}(\omega){\rm d}\omega = \frac{1}{2}\left(\frac{L}{I_1} - \frac{L}{I_3}\right)^{-1}{\rm d}\omega = \frac{1}{2}\frac{{\rm d}\omega}{\Omega} \tag{31}$$

and the nutation angle that corresponds to emission at ω is

$$\theta = \arccos\frac{L/I_1 - \omega}{L/I_1 - L/I_3} = \arccos\left(2 - \frac{\omega}{\Omega}\right). \tag{32}$$

The overall emission spectrum for the $\dot\psi + \dot\phi$ component is then Prob(ω) times the power at this component, equation (25); this is[8]

$$P_{\dot\phi+\dot\psi}(\omega) = \frac{\mu_{\rm ip}^2\omega^4[1 + (L/I_1 - \omega)/(L/I_1 - L/I_3)]^2}{12c^3(L/I_1 - L/I_3)} \tag{33}$$

$$= \frac{\mu_{\rm ip}^2\omega^4\,(3 - \omega/\Omega)^2}{12c^3\Omega}. \tag{34}$$

A similar calculation shows that we obtain the same spectrum from emission at $\dot\phi - \dot\psi$; this is to be expected since the two components are related by the symmetry $\theta \leftrightarrow \pi - \theta$. Thus

$$P_{\dot\phi-\dot\psi}(\omega) = P_{\dot\phi+\dot\psi}(\omega). \tag{35}$$

Following the same procedure, we find that the spectrum emitted at $|\dot\psi|$ is given by

$$P_{|\dot\psi|}(\omega) = \frac{\mu_{\rm ip}^2\omega^4[1 - \omega^2/(L/I_1 - L/I_3)^2]}{3c^3(L/I_1 - L/I_3)} \tag{36}$$

$$= \frac{\mu_{\rm ip}^2\omega^4\left(1 - \omega^2/\Omega^2\right)}{3c^3\Omega} \tag{37}$$

within the range $0 \le \omega \le L/I_1 - L/I_3$, i.e. $0 \le \omega \le \Omega$.

Finally the $\dot\phi$ component is at angular frequency $L/I_1 = 2\Omega$, irrespective of θ. As calculated before, the total power emitted at this frequency is $4\mu_{\rm op}^2(L/I_1)^4/(9c^3)$. Thus, the emitted spectrum is

$$P_{\dot\phi}(\omega) = \frac{4\mu_{\rm op}^2\omega^4}{9c^3}\delta\left(\omega - \frac{L}{I_1}\right) = \frac{4\mu_{\rm op}^2\omega^4}{9c^3}\delta\left(\omega - 2\Omega\right). \tag{38}$$

The total emitted spectrum is then the sum of the four components, equations (34–38), considered only within their respective range of validity. In the particular case of $I_1 = \frac{1}{2}I_3$, we see that $L/I_3 = \Omega, L/I_1 = 2\Omega$ and

$$\begin{aligned} P(\omega|\Omega) = \frac{\omega^4}{c^3}\Bigg\{ &\frac{\mu_{\rm ip}^2}{6\Omega}\left(3 - \frac{\omega}{\Omega}\right)^2\chi_{\Omega<\omega<3\Omega} \\ &+\frac{\mu_{\rm ip}^2}{3\Omega}\left(1 - \frac{\omega^2}{\Omega^2}\right)\chi_{\omega<\Omega} \\ &+\frac{4}{9}\mu_{\rm op}^2\delta(\omega - 2\Omega)\Bigg\}, \end{aligned} \tag{39}$$

where the truth function χ is 1 if the subscripted inequality holds and 0 otherwise. The total power emitted per grain is then

$$\dot E_{\rm spdust} = \frac{2\Omega^4}{3c^3}\left(5\mu_{\rm ip}^2 + \frac{32}{3}\mu_{\rm op}^2\right). \tag{40}$$

This should be compared to $2\Omega^4\mu_{\rm ip}^2/(3c^3)$ for the case of a grain rotating around the $\hat{\boldsymbol{k}}$-axis; for an in-plane dipole moment ($\mu_{\rm op} = 0$) the emitted power is five times higher, whereas for an isotropically distributed dipole moment ($\mu_{\rm ip}^2 : \mu_{\rm op}^2 = 2:1$) the emitted power is $\sim$10 times higher.

[8] Note that $P(\omega)$ has units of erg per second per (radian per second) per grain.

The emissivity per H atom j_ν (units of erg s^{-1} Hz^{-1} sr^{-1} per H atom) can then be obtained by integrating over the probability distribution for Ω and the grain size distribution:

$$\begin{aligned} j_\nu &= \frac{1}{2}\int {\rm d}a\frac{1}{n_{\rm H}}\frac{{\rm d}n_{\rm gr}}{{\rm d}a}\int {\rm d}\Omega P(\omega|\Omega)4\pi\Omega^2 f_a(\Omega) \\ &= \frac{1}{2}\frac{\omega^4}{c^3}\int {\rm d}a\frac{1}{n_{\rm H}}\frac{{\rm d}n_{\rm gr}}{{\rm d}a} \\ &\quad\times\Bigg\{\frac{\mu_{\rm ip}^2}{6}\int_{\frac{\omega}{3}}^{\omega}\frac{{\rm d}\Omega}{\Omega}\left(3 - \frac{\omega}{\Omega}\right)^2 4\pi\Omega^2 f_a(\Omega) \\ &\quad+\frac{\mu_{\rm ip}^2}{3}\int_{\omega}^{\infty}\frac{{\rm d}\Omega}{\Omega}\left(1 - \frac{\omega^2}{\Omega^2}\right)4\pi\Omega^2 f_a(\Omega) \\ &\quad+\frac{2\mu_{\rm op}^2}{9}\pi\omega^2 f_a\left(\frac{\omega}{2}\right)\Bigg\}, \end{aligned} \tag{41}$$

where $\omega = 2\pi\nu$ and the factor $1/2$ comes from multiplying by $2\,\pi$ (conversion from ω to ν) and dividing by 4π (per steradian).

4.2 Radiation–reaction torque

We also need the torque $-\boldsymbol{T}_{\rm rad}$ radiated by the tumbling dipole. This radiation backreacts on the grain, applying a radiation–reaction torque $+\boldsymbol{T}_{\rm rad}$. The general formula for this torque is

$$\boldsymbol{T}_{\rm rad} = -\frac{2}{3c^3}\langle\dot{\boldsymbol{\mu}}\times\ddot{\boldsymbol{\mu}}\rangle, \tag{42}$$

where $\langle ...\rangle$ denotes a time average. Since the rotation of a rigid solid body is quasi-periodic, this amounts to first an average over ϕ and ψ; and in our case, also an average over $\cos\theta$ because of the rapid redistribution of the nutation angle. Averaging over ϕ immediately implies that the x and y components of $\boldsymbol{T}_{\rm rad}$ vanish; the z-component is, after extensive but straightforward manipulation of trigonometric functions,

$$\begin{aligned} T_{{\rm rad},z} = \frac{L^3}{24c^3I_1^3I_3^3}\Big\{ &-3(2I_1^3 + I_1^2I_3 + I_3^3)\mu_{\rm ip}^2 - 8I_3^3\mu_{\rm op}^2 \\ &+\Big[-8I_1^3\mu_{\rm ip}^2 + 4I_3^3(\mu_{\rm ip}^2 + 2\mu_{\rm op}^2)\Big]\cos 2\theta \\ &-(I_1 - I_3)^2(2I_1 + I_3)\mu_{\rm ip}^2\cos 4\theta\Big\}. \end{aligned} \tag{43}$$

Averaging over nutation angles (by multiplying by $\frac{1}{2}\sin\theta$ and integrating over $0 < \theta < \pi$) gives

$$T_{{\rm rad},z} = \frac{-2L^3(3I_1^3 + 3I_1^2I_3 + 4I_3^3)\mu_{\rm ip}^2 + 20L^3I_3^3\mu_{\rm op}^2}{45I_1^3I_3^3c^3}. \tag{44}$$

The case of interest here is $I_1 = \frac{1}{2}I_3$, for which

$$T_{{\rm rad},z} = -\frac{\Omega^3}{c^3}\left(\frac{82}{45}\mu_{\rm ip}^2 + \frac{32}{9}\mu_{\rm op}^2\right). \tag{45}$$

This compares with $-2\Omega^3\mu_{\rm ip}^2/(3c^3)$ for the uniformly rotating case.

We note that equation (45) can also be obtained semi-classically by noting that the photons emitted in the $\dot\phi$ and $\dot\phi \pm \dot\psi$ frequencies carry z angular momentum of $+\hbar$ per photon, while those emitted at the $|\dot\psi|$ frequency carry no z angular momentum.[9] The ratio of angular momentum radiated to energy radiated is

[9] This can be seen by observing that the dipole components at frequencies $\dot\phi$ and $\dot\phi \pm \dot\psi$ are rotating in the xy-plane, while that at $|\dot\psi|$ is oscillating along the z-axis.

thus ω^{-1} for the $\dot{\phi}$ and $\dot{\phi} \pm \dot{\psi}$ components, and we could have written

$$T_{\mathrm{rad},z} = -\int \omega^{-1} P_{\dot{\phi},\dot{\phi}\pm\dot{\psi}}(\omega)\mathrm{d}\omega. \tag{46}$$

This argument, combined with equation (39), confirms equation (45).

Radiation–reaction is implemented in SpDust using the electric dipole damping time τ_{ed}, defined by DL98b to be the radiation–reaction damping time $L/(2|T_{\mathrm{rad},z}|)$ for a grain rotating at thermal velocity, i.e. with rotational kinetic energy $\frac{3}{2}kT$, about the axis of greatest inertia. Mathematically:

$$\left.\frac{\mathrm{d}\Omega}{\mathrm{d}t}\right|_{\mathrm{rad-reac}} = -\frac{I_3\Omega^3}{3kT\tau_{\mathrm{ed}}}. \tag{47}$$

Our calculation establishes that the damping time for planar axisymmetric grains is

$$\tau_{\mathrm{ed}} = \frac{I_3^2 c^3}{3kT}\left(\frac{82}{45}\mu_{\mathrm{ip}}^2 + \frac{32}{9}\mu_{\mathrm{op}}^2\right)^{-1}. \tag{48}$$

5 PLASMA EXCITATION AND DRAG

Plasma excitation is the random torquing of dust grains via their interaction with passing ions; plasma drag is the related effect in which a rotating grain spins down by transferring its angular momentum to the surrounding plasma. These processes have been previously computed for uniformly rotating grains in several papers (Anderson & Watson 1993; DL98b; AHD09).

We consider first the excitation in terms of the power spectrum of the electric field at the position of the grain. Then, we consider the drag, which is determined using detailed balance arguments. Finally, we combine this with the analysis of ion trajectories by AHD09 to obtain the plasma F and G coefficients.

5.1 Excitation in terms of electric field power spectrum

The (nutation angle dependent) plasma excitation coefficient is given by the usual Fokker–Planck rule,

$$I_3^2 E_\parallel(\Omega,\theta)\Delta t = \langle \Delta L_z^2\rangle. \tag{49}$$

This may be evaluated to first order in perturbation theory by noting that the change in z angular momentum in time Δt is equal to the integral of the dipole torque,

$$\Delta L_z = \int_0^{\Delta t} (\mu_x E_y - \mu_y E_x)\mathrm{d}t, \tag{50}$$

where $\boldsymbol{E}$ is the ambient electric field. In terms of the rotation matrix $\mathbf{U}$,

$$\begin{aligned}\Delta L_z = {} & \mu_{\mathrm{ip}}\int_0^{\Delta t}(U_{xi}E_y - U_{yi}E_x)\mathrm{d}t \\ & +\mu_{\mathrm{op}}\int_0^{\Delta t}(U_{xk}E_y - U_{yk}E_x)\mathrm{d}t.\end{aligned} \tag{51}$$

Then the excitation coefficient is

$$\begin{aligned}I_3^2 E_\parallel(\Omega,\theta) = {} & \frac{1}{\Delta t}\Big\langle \mu_{\mathrm{ip}}^2\int_0^{\Delta t}(U_{xi}E_y - U_{yi}E_x)_t\mathrm{d}t \\ & \times\int_0^{\Delta t}(U_{xi}E_y - U_{yi}E_x)_{t'}\mathrm{d}t' \\ & +\mu_{\mathrm{op}}^2\int_0^{\Delta t}(U_{xk}E_y - U_{yk}E_x)_t\mathrm{d}t \\ & \times\int_0^{\Delta t}(U_{xk}E_y - U_{yk}E_x)_{t'}\mathrm{d}t' \\ & +2\mu_{\mathrm{ip}}\mu_{\mathrm{op}}\int_0^{\Delta t}(U_{xi}E_y - U_{yi}E_x)_t\mathrm{d}t \\ & \times\int_0^{\Delta t}(U_{xk}E_y - U_{yk}E_x)_{t'}\mathrm{d}t'\Big\rangle.\end{aligned} \tag{52}$$

To simplify this, we need to change variables to $\tau = t - t'$ and define the inertial frame electric field correlation function by

$$C_{\mathrm{E}}(\tau) = \langle E_x(t)E_x(t')\rangle = \langle E_y(t)E_y(t')\rangle; \tag{53}$$

the xx and yy correlation functions are equal by isotropy of the plasma, and the mixed components are uncorrelated, e.g. $\langle E_y(t)\,E_x(t')\rangle = 0$. We further assume that $C_{\mathrm{E}}(\tau) \to 0$ at sufficiently long lag times τ, which is appropriate for a thermalized isotropic plasma. Then, if Δt is long compared to the decorrelation time (as required for the Fokker–Planck equation to be valid), equation (52) simplifies to

$$\begin{aligned}I_3^2 E_\parallel(\Omega,\theta) = {} & \int_{-\infty}^{\infty}\mathrm{d}\tau\, C_{\mathrm{E}}(\tau) \\ & \times\Big\{\mu_{\mathrm{ip}}^2\langle U_{xi}(t)U_{xi}(t') + U_{yi}(t)U_{yi}(t')\rangle \\ & +\mu_{\mathrm{op}}^2\langle U_{xk}(t)U_{xk}(t') + U_{yk}(t)U_{yk}(t')\rangle \\ & +2\mu_{\mathrm{ip}}\mu_{\mathrm{op}}\langle U_{xi}(t)U_{xk}(t') + U_{yi}(t)U_{yk}(t')\rangle\Big\}.\end{aligned} \tag{54}$$

Note that to obtain this equation we used the fact that to lowest order, the electric field and the grain orientation are independent, so expressions of the type $\langle E_y(t)\,E_y(t')\,U_{xi}(t)\,U_{xi}(t')\rangle$ can be factored into $\langle E_y(t)\,E_y(t')\rangle\,\langle U_{xi}(t)\,U_{xi}(t')\rangle$.

We now perform the angle (ϕ, ψ) averages of the correlation functions of the $\mathbf{U}$ matrix elements using their explicit expressions from equation (21); for example,

$$\begin{aligned}\langle U_{xk}(t)U_{xk}(t')\rangle &= \sin^2\theta\langle\sin\phi(t)\sin\phi(t')\rangle \\ &= \sin^2\theta\langle\sin\phi(t)\sin[\phi(t) - \dot{\phi}\tau]\rangle \\ &= \frac{1}{2}\sin^2\theta\cos(\dot{\phi}\tau).\end{aligned} \tag{55}$$

These simplifications give

$$\begin{aligned}I_3^2 E_\parallel(\Omega,\theta) = {} & \mu_{\mathrm{ip}}^2\int_{-\infty}^{\infty}\mathrm{d}\tau\, C_{\mathrm{E}}(\tau) \\ & \times\left\{\frac{(1-\cos\theta)^2}{4}\cos[(\dot{\phi}-\dot{\psi})\tau]\right. \\ & \left.+\frac{(1+\cos\theta)^2}{4}\cos[(\dot{\phi}+\dot{\psi})\tau]\right\} \\ & +\mu_{\mathrm{op}}^2\int\mathrm{d}\tau\, C_{\mathrm{E}}(\tau)\sin^2\theta\cos(\dot{\phi}\tau).\end{aligned} \tag{56}$$

A further simplification can be achieved by switching from the electric field correlation function to its power spectrum, which is easier to compute. The power spectrum $P_{\mathrm{E}}(f)$ at frequency f is related to the correlation function via

$$\int_{-\infty}^{\infty} C_{\mathrm{E}}(\tau)\cos\omega\tau\,\mathrm{d}\tau = P_{\mathrm{E}}\left(\frac{\omega}{2\pi}\right). \tag{57}$$

This reduces equation (56) to a simple sum,

$$I_3^2 E_\parallel(\Omega,\theta) = \mu_{\rm ip}^2\left\{\frac{(1-\cos\theta)^2}{4}P_{\rm E}\left(\frac{\dot\phi-\dot\psi}{2\pi}\right) + \frac{(1+\cos\theta)^2}{4}P_{\rm E}\left(\frac{\dot\phi+\dot\psi}{2\pi}\right)\right\} + \mu_{\rm op}^2\sin^2\theta\, P_{\rm E}\left(\frac{\dot\phi}{2\pi}\right). \quad (58)$$

The excitation coefficient $E_\parallel(\Omega)$ used in equation (16) can then be obtained by performing the average over nutation angles.

5.2 Plasma drag

The evaluation of the plasma drag is more complicated. In principle, it is a result of second-order perturbation theory: the dipole moment of the grain modifies the trajectories of passing ions, and then the modified charge distribution exerts a torque on the grain with non-zero expectation value.[10] However, a much simpler method of evaluating the plasma drag is to use the principle of detailed balance to relate the rate of small changes in L and θ to the rate of inverse changes. This method works in four stages: first, we need to obtain the diffusion tensor due to plasma drag in (J, K) space (ignoring the thermal spikes); we need to relate the damping rate $\langle\Delta J\rangle$ to the diffusion tensor and then we need to express $\tilde D$ in terms of these coefficients. Finally, we perform the average over nutation angles (or equivalently, over K at fixed J).

5.2.1 Diffusion tensor

The rate of diffusion of a grain in (J, K) space due to plasma excitation is described by a 2×2 symmetric diffusion matrix. We have already computed the component associated with J:

$$E_{JJ} \equiv \frac{{\rm d}\langle\Delta J^2\rangle}{{\rm d}t} = \frac{I_3^2}{\hbar^2}E_\parallel(\Omega,\theta). \quad (59)$$

There are also the other components:

$$E_{JK} \equiv \frac{{\rm d}\langle\Delta J\Delta K\rangle}{{\rm d}t} \quad (60)$$

and

$$E_{KK} \equiv \frac{{\rm d}\langle\Delta K^2\rangle}{{\rm d}t}. \quad (61)$$

We may compute E_{JK} by methods similar to those used to obtain E_{JJ}. The change $\hbar\Delta K$ in the projection of the angular momentum on to the grain $\hat{\boldsymbol{k}}$-axis is equal to the integral of the projection of the torque on to the $\hat{\boldsymbol{k}}$-axis,[11]

$$\hbar\Delta K = \int \hat{\boldsymbol{k}}\cdot(\boldsymbol{\mu}\times\boldsymbol{E})\,{\rm d}t = \int \mu_{\rm ip}\boldsymbol{E}\cdot\hat{\boldsymbol{j}}\,{\rm d}t. \quad (62)$$

The evaluation of equation (60) gives

$$E_{JK} = \frac{\mu_{\rm ip}^2}{4\hbar^2}\left[(1+\cos\theta)^2 P_{\rm E}\left(\frac{\dot\phi+\dot\psi}{2\pi}\right) - (1-\cos\theta)^2 P_{\rm E}\left(\frac{\dot\phi-\dot\psi}{2\pi}\right)\right]. \quad (63)$$

[10] For the same reason, plasma drag can be thought of as the result of emission of plasma 'waves' whose amplitude is proportional to μ and hence whose angular momentum is proportional to μ^2 (Ragot 2002).

[11] In the second equality here, we have used the triple product identity $\boldsymbol{a}\cdot(\boldsymbol{b}\times\boldsymbol{c}) = \boldsymbol{c}\cdot(\boldsymbol{a}\times\boldsymbol{b})$.

We note that $E_{JK}(J, -K) = -E_{JK}(J, K)$ since the two terms in brackets are switched (recall that if $K\to -K$ then $\theta\to\pi-\theta$ and $\dot\psi\to-\dot\psi$).

A similar technique could also be used to compute E_{KK}; however we will not need E_{KK} in our analysis because this does not enter into the equations for D_J.

5.2.2 Relation to drag

The key to computing plasma drag is the principle of detailed balance. We note that in true thermal equilibrium with the plasma, and in the absence of thermal spikes redistributing K (i.e. we consider only plasma interactions as a mechanism of changing J and K), the probability of being in the (J, K) rotational level is

$$P(J,K)\propto(2J+1)\exp\left[\frac{-\hbar^2J(J+1)}{2I_1kT}\right]\times\exp\left[\frac{\hbar^2(I_1^{-1}-I_3^{-1})K^2}{2kT}\right], \quad (64)$$

with the factor $2J+1$ representing the M-sublevel degeneracy.

We define $\Gamma_{J,K\to J',K'}$ to be the rate at which dust grains in the (J, K) quantum state transition to the (J', K') state due to plasma excitation. We further define the quantum number changes $\Delta J = J' - J$ and $\Delta K = K' - K$, and the mean values $J_* = (J + J')/2$ and $K_* = (K + K')/2$. The principle of detailed balance tells us that

$$\Gamma_{J,K\to J',K'}P(J,K) = \Gamma_{J',K'\to J,K}P(J',K'). \quad (65)$$

Assuming (as appropriate for the Fokker–Planck approximation) that $|\Delta J|, |\Delta K| \ll J$, we find

$$\frac{\Gamma_{J,K\to J',K'}}{\Gamma_{J',K'\to J,K}} = \frac{2J'+1}{2J+1}\exp\left[\frac{-\hbar^2[J'(J'+1)-J(J+1)]}{2I_1kT}\right]\times\exp\left[\frac{\hbar^2(I_1^{-1}-I_3^{-1})}{2kT}(K'^2-K^2)\right] \approx 1+\frac{\Delta J}{J}-\frac{\hbar^2J\Delta J}{I_1kT}+\frac{\hbar^2(I_1^{-1}-I_3^{-1})K\Delta K}{kT}. \quad (66)$$

We then define the symmetrized rate,

$$S_{\Delta J,\Delta K}(J_*,K_*) = \frac{\Gamma_{J,K\to J',K'}+\Gamma_{J',K'\to J,K}}{2}, \quad (67)$$

defined at either integer or half-integer values of the arguments depending on whether ΔJ and ΔK are even or odd. The rate S is symmetric in the sense that $S_{\Delta J,\Delta K}(J_*, K_*) = S_{-\Delta J,-\Delta K}(J_*, K_*)$. Then

$$\Gamma_{J,K\to J',K'} = S_{\Delta J,\Delta K}(J_*,K_*)\left[1+\frac{\Delta J}{2J}-\frac{\hbar^2J\Delta J}{2I_1kT}+\frac{\hbar^2(I_1^{-1}-I_3^{-1})K\Delta K}{2kT}\right]; \quad (68)$$

Taylor-expanding S and keeping only terms first order in ΔJ and ΔK gives

$$\Gamma_{J,K\to J',K'} = S_{\Delta J,\Delta K}(J,K)\left[1+\frac{\Delta J}{2J}-\frac{\hbar^2J\Delta J}{2I_1kT}+\frac{\hbar^2(I_1^{-1}-I_3^{-1})K\Delta K}{2kT}\right]+\frac{\Delta J}{2}\partial_J S_{\Delta J,\Delta K}(J,K)+\frac{\Delta K}{2}\partial_K S_{\Delta J,\Delta K}(J,K). \quad (69)$$

We may now relate the excitation rates to the symmetrized rate function. Inspection of equation (59) gives

$$E_{JJ}(J,K) = \sum_{\Delta J\Delta K} \Delta J^2 \Gamma_{J,K\to J',K'} = \sum_{\Delta J\Delta K} \Delta J^2 S_{\Delta J,\Delta K}(J,K), \tag{70}$$

and similarly for E_{JK} and E_{KK}. We may then investigate the mean rate of change of J:

$$\frac{\mathrm{d}\langle\Delta J\rangle}{\mathrm{d}t} = \sum_{\Delta J\Delta K} \Delta J\ \Gamma_{J,K\to J',K'}. \tag{71}$$

Here, the contributions from ΔJ, ΔK and $-\Delta J$, $-\Delta K$ nearly cancel. They differ only due to the presence of first-order terms (in ΔJ, ΔK) in equation (69); these give

$$\begin{aligned}\frac{\mathrm{d}\langle\Delta J\rangle}{\mathrm{d}t} &= \sum_{\Delta J\Delta K} \Delta J\left[\left(\frac{\Delta J}{2J} - \frac{\hbar^2 J\Delta J}{2I_1 kT} + \frac{\hbar^2(I_1^{-1}-I_3^{-1})K\Delta K}{2kT}\right)S_{\Delta J,\Delta K} + \frac{\Delta J}{2}\partial_J S_{\Delta J,\Delta K}(J,K) + \frac{\Delta K}{2}\partial_K S_{\Delta J,\Delta K}(J,K)\right] \\ &= \left(\frac{1}{2J} - \frac{\hbar^2 J}{2I_1 kT}\right)E_{JJ} + \frac{\hbar^2(I_1^{-1}-I_3^{-1})K}{2kT}E_{JK} + \frac{1}{2}\frac{\partial E_{JJ}}{\partial J} + \frac{1}{2}\frac{\partial E_{JK}}{\partial K}.\end{aligned} \tag{72}$$

We thus arrive at the remarkable result that the rate of loss of angular momentum due to plasma drag is expressible in terms of E_{JJ} and E_{JK}. Equation (72) is the closest that we come to a standard fluctuation–dissipation relation.

5.2.3 Computation of the drag coefficient $\tilde{D}$

In order to continue, we recall that we ultimately need the function $\tilde{D}(\Omega)$, which first requires us to find $D(\Omega,\theta)$ and its average over nutation angles $D(\Omega)$. We recall that

$$D(\Omega,\theta) = -\frac{\mathrm{d}\langle\Delta\boldsymbol{\Omega}\rangle}{\mathrm{d}t}\cdot\hat{\boldsymbol{e}}_{\boldsymbol{\Omega}}. \tag{73}$$

This is *not* the same as

$$-\frac{\mathrm{d}\langle\Delta\Omega\rangle}{\mathrm{d}t} = -\frac{\hbar}{I_3}\frac{\mathrm{d}\langle\Delta J\rangle}{\mathrm{d}t}, \tag{74}$$

where '$\Delta\Omega$' is understood as $\Delta|\boldsymbol{\Omega}|$ and the last equality holds in the large J limit. These two quantities are however related:

$$\begin{aligned}\Delta\Omega &= |\boldsymbol{\Omega}+\Delta\boldsymbol{\Omega}| - |\boldsymbol{\Omega}| \\ &= \sqrt{\Omega^2 + 2\Delta\boldsymbol{\Omega}\cdot\boldsymbol{\Omega} + (\Delta\boldsymbol{\Omega})^2} - \Omega \\ &= \Omega\left[\frac{\Delta\boldsymbol{\Omega}\cdot\boldsymbol{\Omega}}{\Omega^2} + \frac{(\Delta\boldsymbol{\Omega})^2}{2\Omega^2} - \frac{1}{8}\left(\frac{2\Delta\boldsymbol{\Omega}\cdot\boldsymbol{\Omega}}{\Omega^2}\right)^2 + \mathcal{O}\left(\frac{\Delta\boldsymbol{\Omega}}{\Omega}\right)^3\right].\end{aligned} \tag{75}$$

Averaging and taking the time derivative implies

$$\frac{\mathrm{d}\langle\Delta\Omega\rangle}{\mathrm{d}t} = \frac{\mathrm{d}\langle\Delta\boldsymbol{\Omega}\rangle}{\mathrm{d}t}\cdot\hat{\boldsymbol{e}}_{\boldsymbol{\Omega}} + \frac{E_\perp(\Omega,\theta)}{\Omega}, \tag{76}$$

where the parallel part of the excitation was cancelled by the third term in equation (75). Solving for D then gives

$$D(\Omega,\theta) = -\frac{\hbar}{I_3}\frac{\mathrm{d}\langle\Delta J\rangle}{\mathrm{d}t} + \frac{E_\perp(\Omega,\theta)}{\Omega}, \tag{77}$$

and averaging over the nutation angle, or equivalently over K, gives the coefficient used in the Fokker–Planck equation:

$$D(\Omega) = -\frac{\hbar}{I_3}\left\langle\frac{\mathrm{d}\langle\Delta J\rangle}{\mathrm{d}t}\right\rangle_K + \frac{E_\perp(\Omega)}{\Omega}. \tag{78}$$

The modified damping coefficient $\tilde{D}(\Omega)$ of equation (17) is then

$$\tilde{D} = -\frac{\hbar}{I_3}\left\langle\frac{\mathrm{d}\langle\Delta J\rangle}{\mathrm{d}t}\right\rangle_K + \frac{E_\parallel}{\Omega} + \frac{1}{2}\frac{\mathrm{d}E_\parallel}{\mathrm{d}\Omega}, \tag{79}$$

or in terms of J, and using the averaged equation (59) $E_\parallel = \frac{\hbar^2}{I_3^2}\langle E_{JJ}\rangle_K$, we have

$$\frac{I_3}{\hbar}\tilde{D} = -\left\langle\frac{\mathrm{d}\langle\Delta J\rangle}{\mathrm{d}t}\right\rangle_K + \frac{\langle E_{JJ}\rangle_K}{J} + \frac{1}{2}\frac{\mathrm{d}}{\mathrm{d}J}\langle E_{JJ}\rangle_K. \tag{80}$$

Here, the averages are taken over the nutation quantum number K. It is critical to note here that $\mathrm{d}/\mathrm{d}J$ is a *total* derivative, i.e. the averaging over K is understood to take place *before* the differentiation. This is because in the definition (equation 17), $\tilde{D}$ is ultimately constructed out of drift and diffusion coefficients $\boldsymbol{D}$ and $\mathbf{E}$ that have already been K-averaged. Thus we *cannot* replace the last term with the average of a partial derivative, $\langle\partial E_{JJ}/\partial J\rangle_K$.

Equation (80) may be simplified by plugging in equation (72):

$$\frac{I_3}{\hbar}\tilde{D} = \left(\frac{1}{2J} + \frac{\hbar^2 J}{2I_1 kT}\right)\langle E_{JJ}\rangle_K - \frac{\hbar^2(I_1^{-1}-I_3^{-1})}{2kT}\langle K E_{JK}\rangle_K - \frac{1}{2}\left\langle\frac{\partial E_{JJ}}{\partial J}\right\rangle_K - \frac{1}{2}\left\langle\frac{\partial E_{JK}}{\partial K}\right\rangle_K + \frac{1}{2}\frac{\mathrm{d}}{\mathrm{d}J}\langle E_{JJ}\rangle_K. \tag{81}$$

5.2.4 Nutation angle average

Our final step in the above analysis is to perform the average over nutation states K. We would like to express equation (81) in a form that does not contain any derivatives, since the latter tend to be numerically unstable. We begin by making the replacement:

$$\langle\rangle_K \to \frac{1}{2J}\int_{-J}^{J}\mathrm{d}K, \tag{82}$$

valid for large values of J (i.e. the classical regime). Each of the three derivative-containing terms in equation (81) then simplifies. For example,

$$\left\langle\frac{\partial E_{JK}}{\partial K}\right\rangle_K = \frac{1}{2J}\int_{-J}^{J}\frac{\partial E_{JK}}{\partial K}\mathrm{d}K = \frac{E_{JK}(J,J) - E_{JK}(J,-J)}{2J}. \tag{83}$$

The last term simplifies as well:

$$\frac{\mathrm{d}}{\mathrm{d}J}\langle E_{JJ}\rangle_K = \frac{\mathrm{d}}{\mathrm{d}J}\left(\frac{1}{2J}\int_{-J}^{J}E_{JJ}\mathrm{d}K\right) = -\frac{1}{2J^2}\int_{-J}^{J}E_{JJ}\mathrm{d}K + \frac{1}{2J}\int_{-J}^{J}\frac{\partial E_{JJ}}{\partial J}\mathrm{d}K + \frac{E_{JJ}(J,J)+E_{JJ}(J,-J)}{2J}. \tag{84}$$

By symmetry under change of sign of K (i.e. $\theta \leftrightarrow \pi - \theta$), we have $E_{JK}(J, -J) = -E_{JK}(J, J)$ and $E_{JJ}(J, -J) = E_{JJ}(J, J)$. Also, inspection of equations (58) and (63) in the $K = J$ ($\theta = 0$) case shows that[12] $E_{JJ}(J, J) = E_{JK}(J, J)$. Substituting these results into equation (81), we find a mass cancellation resulting in

$$\frac{I_3}{\hbar}\tilde{D} = \frac{\hbar^2}{4I_1kT}\int_{-J}^{J} E_{JJ}\,\mathrm{d}K - \frac{\hbar^2(I_1^{-1} - I_3^{-1})}{4JkT}\int_{-J}^{J} K E_{JK}\,\mathrm{d}K. \quad (85)$$

The detailed balance-derived drag coefficient can be generalized for any bath at temperature T_X, and can be written in the form:

$$\tilde{D} = \frac{I_3\Omega}{2kT_X}\left[\frac{I_3}{I_1}E_\parallel - \left(\frac{I_3}{I_1} - 1\right)\left\langle \frac{K}{J}\frac{\hbar^2 E_{JK}}{I_3^2}\right\rangle_K\right]. \quad (86)$$

This should be compared to the fluctuation–dissipation theorem, $\tilde{D} = I_3\Omega E_\parallel/2kT_X$, valid for a grain rotating around its axis of greatest inertia. In particular, equation (86) reduces to the fluctuation–dissipation theorem in the limit of spherical grain ($I_3/I_1 = 1$).

5.3 Computation of *G* and *F* coefficients

We are finally ready to construct formulas for the G and F coefficients. It is most convenient to express these in terms of the AHD09 excitation coefficients $G_{\mathrm{p,AHD}}(\Omega)$, which of course have already been calculated. Recall that on account of the fluctuation–dissipation theorem we had $F_{\mathrm{p,AHD}}(\Omega) = G_{\mathrm{p,AHD}}(\Omega)$. In all cases, we set $I_1 = \frac{1}{2}I_3$.

5.3.1 G coefficient

We recall that the AHD09 excitation coefficient was derived by assuming $\theta = 0$, in which case equation (58) reduces to

$$I_3^2 E_\parallel(\Omega; \theta = 0) = \mu_{\mathrm{ip}}^2 P_{\mathrm{E}}\left(\frac{\Omega}{2\pi}\right). \quad (87)$$

The plasma excitation rate, using equation (19), is then

$$G_{\mathrm{p,AHD}}(\Omega) = \frac{\tau_{\mathrm{H}}}{2I_3kT}\mu_{\mathrm{ip}}^2 P_{\mathrm{E}}\left(\frac{\Omega}{2\pi}\right). \quad (88)$$

This allows us to express the electric field power spectrum $P_{\mathrm{E}}(f)$ in terms of the AHD09 excitation coefficients:

$$P_{\mathrm{E}}(f) = \frac{2I_3kT}{\tau_{\mathrm{H}}\mu_{\mathrm{ip}}^2}G_{\mathrm{p,AHD}}(2\pi f). \quad (89)$$

We may now use equation (58) to obtain the plasma excitation rate for general θ. Recalling that $\dot{\phi} = 2\Omega$ and $\dot{\psi} = -\Omega\cos\theta$, we find

$$G_{\mathrm{p}}(\Omega, \theta) = \frac{(1 - \cos\theta)^2}{4}G_{\mathrm{p,AHD}}[(2 + \cos\theta)\Omega] + \frac{(1 + \cos\theta)^2}{4}G_{\mathrm{p,AHD}}[(2 - \cos\theta)\Omega] + \frac{\mu_{\mathrm{op}}^2}{\mu_{\mathrm{ip}}^2}\sin^2\theta\, G_{\mathrm{p,AHD}}(2\Omega). \quad (90)$$

[12] Although we use the plasma drag calculation to prove it, this is a general result. If we start at $K = J$ then a small change $\Delta J - \Delta K = J - K \approx J\Delta\theta^2/2$. Therefore, the combination of diffusion coefficients $E_{JJ} - E_{JK}$ evaluates to $\langle\Delta J(\Delta J - \Delta K)\rangle/\Delta t = J\langle\Delta J\Delta\theta^2\rangle/\Delta t$. But diffusion is a $\Delta t^{1/2}$ process so $\langle\Delta J\Delta\theta^2\rangle$ is at least of order $\Delta t^{3/2}$. Hence, taking the limit as $\Delta t \to 0^+$, $\mathrm{E_{JJ}} - E_{JK}$ vanishes.

We now average over values of $\cos\theta$ between -1 and $+1$. The first two terms give identical contributions, and the last one simplifies using $\langle\sin^2\theta\rangle = \frac{2}{3}$. Thus,

$$G_{\mathrm{p}}(\Omega) = \frac{1}{4}\int_{\Omega}^{3\Omega}\left(3 - \frac{\omega}{\Omega}\right)^2 G_{\mathrm{p,AHD}}(\omega)\frac{\mathrm{d}\omega}{\Omega} + \frac{2\mu_{\mathrm{op}}^2}{3\mu_{\mathrm{ip}}^2}G_{\mathrm{p,AHD}}(2\Omega). \quad (91)$$

5.3.2 F coefficient

A similar technique works for the drag coefficient. We substitute equation (85) for $\tilde{D}$ into equation (18) to obtain an expression for $F_{\mathrm{p}}(\Omega)$. This in turn depends on the excitation coefficients E_{JJ} [from equations (59) and (58)] and E_{JK} [from equation (63)]. This leads to an expression involving electric field power spectra, which we transform into AHD09 coefficients using equation (89). Converting the integrals over K to integrals over $\cos\theta = K/J$ and using $\hbar J = I_3\Omega$, we find a mass cancellation of prefactors, giving

$$F_{\mathrm{p}}(\Omega) = 2G_{\mathrm{p}}(\Omega) - \frac{1}{2}\int_{-1}^{1}\left\{\frac{(1 + \cos\theta)^2}{4}G_{\mathrm{p,AHD}}[(2 - \cos\theta)\Omega] - \frac{(1 - \cos\theta)^2}{4}G_{\mathrm{p,AHD}}[(2 + \cos\theta)\Omega]\right\}\cos\theta\,\mathrm{d}\cos\theta. \quad (92)$$

This simplifies to

$$F_{\mathrm{p}}(\Omega) = \frac{1}{4}\int_{\Omega}^{3\Omega}\frac{\omega}{\Omega}\left(3 - \frac{\omega}{\Omega}\right)^2 G_{\mathrm{p,AHD}}(\omega)\frac{\mathrm{d}\omega}{\Omega} + \frac{4\mu_{\mathrm{op}}^2}{3\mu_{\mathrm{ip}}^2}G_{\mathrm{p,AHD}}(2\Omega). \quad (93)$$

Note that due to the K-averaging there is no longer a definite relation between F and G. However, since $G_{\mathrm{p,AHD}}(\omega) > 0$ for all ω, we find the inequality

$$1 < \frac{F_{\mathrm{p}}(\Omega)}{G_{\mathrm{p}}(\Omega)} < 3. \quad (94)$$

The calculation of $G_{\mathrm{p,AHD}}(\omega)$ is one of the most time-consuming parts of SpDust, but it varies slowly as a function of frequency and is only required over a range of a factor of 3 in frequency ($\Omega < \omega < 3\Omega$). Thus, we implement it with an approximate integrator as described in Appendix A.

We show the plasma excitation and drag coefficient for a grain containing $N_{\mathrm{C}} = 54$ carbon atoms (equivalent radius $a \approx 5$ Å), in WIM conditions (as defined in DL98b) in Fig. 2.

6 INFRARED EXCITATION AND DAMPING

Another major spin-up/down mechanism for the smallest grains is the emission of infrared photons during thermal spikes. Here, we consider the excitation and damping due to these spikes.

The excitation rate is doubled from the AHD09 treatment for *all* grains (spherical or not) due to a previous error associated with the emitted photon angular momentum (the angular momentum carried away by a photon is $\sqrt{2}\,\hbar$ rather than just $\hbar$). This is the only modification in this paper that applies to spherical as well as disc-like grains.

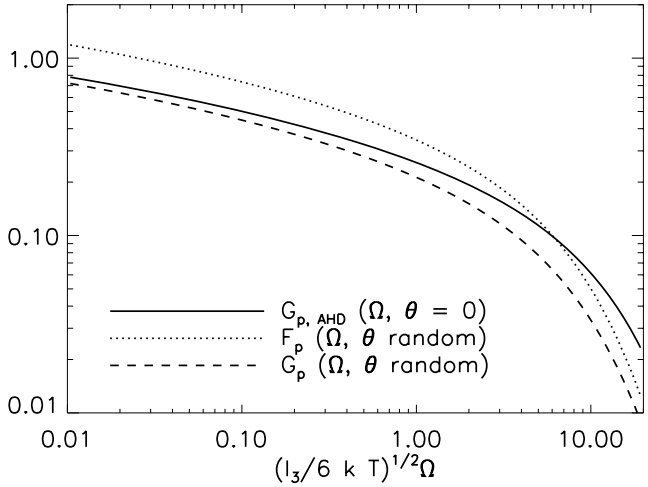

Figure 2. Plasma excitation and drag dimensionless coefficients for $N_C = 54$ in the WIM.

6.1 Excitation

Infrared excitation is the random change in angular momentum resulting from the fact that each infrared photon emitted by the grain carries away some angular momentum. In the previous analyses of DL98b and AHD09, it was assumed that the resulting change in angular momentum had variance $\langle \Delta \boldsymbol{L}^2 \rangle = \hbar^2$ (since a photon carries one quantum of angular momentum), or on one axis $\langle \Delta L_z^2 \rangle = \frac{1}{3}\hbar^2$. In fact, the excitation is twice this as can be seen from either of the following arguments:

(i) an electric dipole photon has angular momentum quantum number $j = 1$, so if it carries off angular momentum $-\Delta \boldsymbol{L}$ (thereby imparting $\Delta \boldsymbol{L}$ to the grain via back-reaction), we have $\Delta \boldsymbol{L}^2 = j(j+1)\hbar^2 = 2\hbar^2$.

(ii) the z-component of the angular momentum of the photon is $\Delta L_z = -m\hbar$, where $m \in \{-1, 0, 1\}$ is the azimuthal quantum number of the emitted photon. Since these three possibilities are equally likely for an isotropically oriented grain, we see that $\langle \Delta L_z^2 \rangle = \frac{2}{3}\hbar^2$.

Both of these arguments show that the infrared excitation $G_{\rm IR}$ is twice that reported in AHD09, i.e.

$$G_{\rm IR} = \frac{h\tau_{\rm H}}{3\pi I_3 kT} \int_0^\infty \frac{F_\nu}{\nu}\, {\rm d}\nu, \tag{95}$$

where F_ν is the spectrum of infrared radiation emitted by the grain (in e.g. erg s^{-1} Hz^{-1} sr^{-1}).

The correct excitation rate *was* included in Ysard & Verstraete (2009), however their formalism is quite different (e.g. they use J rather than Ω as the independent variable) and so the discrepancy appears to have not been noticed previously.

6.2 Damping

We next consider the infrared damping rate, which arises due to slight preferential emission of positive over negative angular momentum photons from a rotating grain. A classical model of the effect can be constructed by considering oscillators either in the plane of the grain or out of the plane. The torque from an isotropic distribution of oscillators would correspond to adding $\frac{2}{3}$ of the in-plane and $\frac{1}{3}$ of the out-of-plane result.

We consider an oscillating dipole $\boldsymbol{p}$ with angular frequency $\omega = 2\pi\nu$ and amplitude P. In the out-of-plane case, this corresponds to a dipole moment:

$$\begin{aligned} \boldsymbol{p} &= P\sin(\omega t)\,\hat{\boldsymbol{k}} \\ &= P\sin(\omega t)(\sin\theta\sin\phi, -\sin\theta\cos\phi, \cos\theta). \end{aligned} \tag{96}$$

The torque on the grain is then

$$\boldsymbol{T} = -\frac{2}{3c^3}\langle \dot{\boldsymbol{p}} \times \ddot{\boldsymbol{p}} \rangle, \tag{97}$$

where the derivatives are taken in the inertial frame. The evaluation of the time average of the z-component of the torque is then a straightforward exercise; to the lowest order in $\dot{\phi}$, we find

$$T_z^{\rm op} = -\frac{\omega^2 P^2 \sin^2\theta}{c^3}\dot{\phi}. \tag{98}$$

A similar exercise for an in-plane oscillator gives

$$\begin{aligned} T_z^{\rm ip} = -\frac{\omega^2 P^2}{4c^3}\Big[&(1+\cos\theta)^2(\dot{\phi}+\dot{\psi}) \\ &+(1-\cos\theta)^2(\dot{\phi}-\dot{\psi})\Big]. \end{aligned} \tag{99}$$

If we average these over nutation angles, we get

$$\langle T_z^{\rm op}\rangle_\theta = -\frac{4\omega^2 P^2}{3c^3}\Omega \tag{100}$$

and

$$\langle T_z^{\rm ip}\rangle_\theta = -\frac{\omega^2 P^2}{c^3}\Omega. \tag{101}$$

In order to calculate damping coefficients, we must sum over all the oscillators P that contribute to the infrared emission. The total power emitted by this dipole is

$$4\pi F_\nu = \frac{\omega^4 P^2}{3c^3}\delta\left(\nu - \frac{\omega}{2\pi}\right), \tag{102}$$

so we make the replacement:

$$P^2 \to \int_0^\infty {\rm d}\nu\, \frac{12\pi c^3}{\omega^4} F_\nu = \int_0^\infty {\rm d}\nu\, \frac{3c^3}{\pi\omega^2\nu^2} F_\nu, \tag{103}$$

with $\omega = 2\pi\nu$. The total torque is then

$$T = -\int_0^\infty {\rm d}\nu\, \frac{\Omega}{\pi\nu^2}(3F_\nu^{\rm ip} + 4F_\nu^{\rm op}), \tag{104}$$

where $F_\nu^{\rm ip}$ and $F_\nu^{\rm op}$ are the emission spectra contributed by the in-plane and out-of-plane modes. The damping coefficient is

$$F_{\rm IR} = \frac{\tau_{\rm H}}{\pi I_3}\int_0^\infty {\rm d}\nu\, \frac{3F_\nu^{\rm ip} + 4F_\nu^{\rm op}}{\nu^2}. \tag{105}$$

We can see that there is very little difference between the in-plane and out-of-plane mode contributions (a factor of $\frac{4}{3}$). Assuming the isotropic case where $\frac{2}{3}$ of the emission is in-plane and $\frac{1}{3}$ is out-of-plane,[13] we find

$$F_{\rm IR} = \frac{10\tau_{\rm H}}{3\pi I_3}\int_0^\infty \frac{F_\nu}{\nu^2}\, {\rm d}\nu. \tag{106}$$

This is $\frac{5}{3}$ times the AHD09 damping coefficient for spherical grains.

[13] In the case of the PAH bands, it is known that some bands correspond to in-plane vibrations and some to out-of-plane; however given the small difference between the two cases, we have not tracked them separately.

7 COLLISIONS

Collisions of dust grains break down into several cases: the grain may be charged or neutral, and the impactor may be ionized or neutral. Furthermore, one must consider not just the angular momentum imparted by the incoming particle, but also how much angular momentum it carries away when it evaporates. We denote the damping and excitation rates with subscripts 'i' or 'n' (for ion or neutral impactor) and superscripts '(in)' or '(ev)' for incoming or evaporative contributions. In the $\theta = 0$ case, the grain's geometry is time-stationary in the inertial frame, and incoming particles are equally likely to impact the grain whether they approach on prograde or retrograde trajectories, and hence $F^{(\mathrm{in})} = 0$. For the more general case, there will be a new $F_{\mathrm{n}}^{(\mathrm{in})}$ contribution associated with the fact that the grain can physically crash into passing particles, and this leads to a preference to accrete incoming particles on retrograde orbits.

The general problem is not tractable analytically, so we focus first on the case of neutral impactors on neutral grains. We then heuristically extend the calculation to the more general case.

7.1 Damping rate: neutral grains, neutral impactors

There are two contributions to the damping rate. The first is the evaporative damping, $F_{\mathrm{coll}}^{(\mathrm{ev})}$, which arises because particles evaporating off the grain surface preferentially have positive L_z. The second is a new contribution, $F_{\mathrm{coll}}^{(\mathrm{in})}$, which arises because a grain rotating around an axis other than a symmetry axis preferentially collides with incoming particles of negative L_z. We consider both in turn. In both cases, we assume the grain to be a convex rigid body whose surface area element is d S, whose normal vector is $\hat{\boldsymbol{n}}$ and whose instantaneous angular velocity is $\boldsymbol{\omega}$.

7.1.1 Evaporation

We suppose that a particle evaporates from position $\boldsymbol{r}$ on the grain surface. This point has a local surface velocity $\boldsymbol{v}_0 = \boldsymbol{\omega} \times \boldsymbol{r}$. The local phase-space density of particles evaporating from the grain surface is

$$f(\boldsymbol{r}, \boldsymbol{v}) = K \exp\left[-\frac{m(\boldsymbol{v} - \boldsymbol{v}_0)^2}{2kT_{\mathrm{ev}}}\right], \tag{107}$$

for $\boldsymbol{v}$ in the half-space:

$$\mathcal{H} \equiv \{\boldsymbol{v} \in \mathbb{R}^3 : (\boldsymbol{v} - \boldsymbol{v}_0) \cdot \hat{\boldsymbol{n}} > 0\}. \tag{108}$$

The normalization constant K can be found from the requirement that the rate of collisions per unit area is equal to the rate of evaporation per unit area. The flux of evaporating particles (in particles cm^{-2} s^{-1}) is obtained by integrating $(\boldsymbol{v} - \boldsymbol{v}_0) \cdot \hat{\boldsymbol{n}} f$ over $\mathcal{H}$, giving

$$\frac{\pi}{2}\left(\frac{2kT_{\mathrm{ev}}}{m}\right)^2 K = \frac{1}{S}\frac{\mathrm{d}N_{\mathrm{coll}}}{\mathrm{d}t}. \tag{109}$$

The angular momentum imparted to the grain by an individual escaping atom is obtained from Newton's third law, $\Delta\boldsymbol{L} = -m\,\boldsymbol{r} \times \boldsymbol{v}$. For an ensemble of escaping atoms, we should write

$$\frac{\mathrm{d}\langle\Delta\boldsymbol{L}\rangle}{\mathrm{d}t} = m \oint \mathrm{d}S \int_{\mathcal{H}} \mathrm{d}^3\boldsymbol{v}(-\boldsymbol{r} \times \boldsymbol{v})[(\boldsymbol{v} - \boldsymbol{v}_0) \cdot \hat{\boldsymbol{n}}] f(\boldsymbol{r}, \boldsymbol{v}). \tag{110}$$

The velocity integral is straightforwardly evaluated using the substitution $\boldsymbol{v} = \boldsymbol{v}_0 + \boldsymbol{u}$. The result is

$$\frac{\mathrm{d}\langle\Delta\boldsymbol{L}\rangle}{\mathrm{d}t} = mK \oint \mathrm{d}S \left[-(\boldsymbol{r} \times \boldsymbol{v}_0)2\pi\left(\frac{kT_{\mathrm{ev}}}{m}\right)^2 - \int_{\boldsymbol{u}\cdot\hat{\boldsymbol{n}}>0} (\boldsymbol{r} \times \boldsymbol{u})(\boldsymbol{u} \cdot \hat{\boldsymbol{n}})\mathrm{e}^{-mu^2/2kT_{\mathrm{ev}}}\mathrm{d}^3\boldsymbol{u}\right]. \tag{111}$$

The second integral has an integrand even in $\boldsymbol{u}$, so its value is exactly $\frac{1}{2}$ of the integral extended over all $\boldsymbol{u} \in \mathbb{R}^3$. The resulting integrand is then a quadratic function of the components of $\boldsymbol{u}$ times a Gaussian. Such integrals are easily evaluated; in this case, the result is proportional to $\boldsymbol{r} \times \hat{\boldsymbol{n}}$.[14] But we know that $\oint \boldsymbol{r} \times \hat{\boldsymbol{n}}\,\mathrm{d}S = 0$ for any closed surface, so the second integral vanishes.[15] Therefore, we keep only the first integral. Using $\boldsymbol{v}_0 = \boldsymbol{\Omega} \times \boldsymbol{r}$, we reduce equation (111) to

$$\frac{\mathrm{d}\langle\Delta\boldsymbol{L}\rangle}{\mathrm{d}t} = -\frac{m}{S}\frac{\mathrm{d}N_{\mathrm{coll}}}{\mathrm{d}t} \oint \boldsymbol{r} \times (\boldsymbol{\omega} \times \boldsymbol{r})\,\mathrm{d}S. \tag{112}$$

In the particular case of a disc-like grain of uniform and infinitesimal thickness, the surface average of $\boldsymbol{r} \times (\boldsymbol{\omega} \times \boldsymbol{r})$ is the same as its volume average, which by inspection is the angular momentum $\boldsymbol{L}$ divided by the grain mass M. Thus,

$$\frac{\mathrm{d}\langle\Delta\boldsymbol{L}\rangle}{\mathrm{d}t} = -\frac{m}{M}\frac{\mathrm{d}N_{\mathrm{coll}}}{\mathrm{d}t}\boldsymbol{L}, \tag{113}$$

or

$$D(\Omega) = \frac{m}{M}\frac{\mathrm{d}N_{\mathrm{coll}}}{\mathrm{d}t}. \tag{114}$$

This does not depend on θ, so the evaporation contribution to the damping is not modified from the principal axis case. The relation

$$F_{\mathrm{n}}^{(\mathrm{ev})} = \frac{n_{\mathrm{n}}}{n_{\mathrm{H}}}\sqrt{\frac{m_{\mathrm{n}}}{m_{\mathrm{H}}}} \tag{115}$$

for neutral atoms impacting neutral grains remains valid.

7.1.2 Incoming particles

We now require the angular momentum acquired from incoming particles. This is actually very similar to the previous calculation, except that the phase-space density of incoming atoms has zero net velocity,

$$f(\boldsymbol{r}, \boldsymbol{v}) = n\left(\frac{m}{2\pi kT}\right)^{3/2} \exp\left(-\frac{mv^2}{2kT}\right), \tag{116}$$

and the relevant region of velocity space is now the complement of $\mathcal{H}$, i.e. $\mathcal{H}^{\mathrm{c}}$. The angular momentum transfer rate is

$$\frac{\mathrm{d}\langle\Delta\boldsymbol{L}\rangle}{\mathrm{d}t} = m \oint \mathrm{d}S \int_{\mathcal{H}^{\mathrm{c}}} \mathrm{d}^3\boldsymbol{v}\,(\boldsymbol{r} \times \boldsymbol{v})[-(\boldsymbol{v} - \boldsymbol{v}_0) \cdot \hat{\boldsymbol{n}}] f(\boldsymbol{r}, \boldsymbol{v}). \tag{117}$$

We now Taylor-expand to first order in $\boldsymbol{v}_0$. The zeroth-order term (i.e. for $\boldsymbol{v}_0 = \boldsymbol{0}$) is proportional to $\oint \boldsymbol{r} \times \hat{\boldsymbol{n}}\,\mathrm{d}S = 0$ and vanishes. There are two possible contributions to the first-order term. One arises from the explicit $\boldsymbol{v}_0$ in the integrand. The other arises from

[14] This can be seen from symmetry, since the integral must be linear in $\boldsymbol{r}$ and $\hat{\boldsymbol{n}}$, and has the symmetry of a pseudo-vector.

[15] This is based on the assumption that the evaporation properties (e.g. T_{ev}) are uniform across the grain surface. If this is violated, e.g. by catalytic sites for the formation of H_2, then there can be a systematic torque. This has been previously investigated and found to be negligible for the smallest grains (DL98b).

the dependence of the integration region $\mathcal{H}^{\rm c}$ on $\boldsymbol{v}_0$. That is, to the first order in $\boldsymbol{v}_0$,

$$\frac{{\rm d}\langle\Delta \boldsymbol{L}\rangle}{{\rm d}t} = m \oint {\rm d}S \left[\int_{\mathcal{H}^{\rm c}} {\rm d}^3\boldsymbol{v}\, (\boldsymbol{r}\times\boldsymbol{v})(\boldsymbol{v}_0\cdot\hat{\boldsymbol{n}})\, f(\boldsymbol{r},\boldsymbol{v}) + \int_{\partial\mathcal{H}^{\rm c}} {\rm d}^2\boldsymbol{v}\, (\boldsymbol{v}_0\cdot\hat{\boldsymbol{n}})(\boldsymbol{r}\times\boldsymbol{v})(-\boldsymbol{v}\cdot\hat{\boldsymbol{n}})\, f(\boldsymbol{r},\boldsymbol{v}) \right], \quad (118)$$

where the integration region $\mathcal{H}^{\rm c}$ is evaluated at $\boldsymbol{v}_0 = \boldsymbol{0}$; $\partial\mathcal{H}^{\rm c}$ is the boundary of $\mathcal{H}^{\rm c}$ and ${\rm d}^2\boldsymbol{v}$ is the area element on the boundary. The boundary at non-zero $\boldsymbol{v}_0$ is displaced a distance $\boldsymbol{v}_0\cdot\hat{\boldsymbol{n}}$, hence the inclusion of this factor in the second term, combined with the area element ${\rm d}^2\boldsymbol{v}$, is the element of volume that is brought inside $\mathcal{H}^{\rm c}$ due to non-zero $\boldsymbol{v}_0$.[16] The second term can be seen to vanish because $\boldsymbol{v}\cdot\hat{\boldsymbol{n}} = 0$ on the boundary $\partial\mathcal{H}^{\rm c}$. Therefore this second term may be dropped.

Using the Maxwellian distribution, we may perform the velocity integral in the first (surviving) term in equation (118) to get

$$\frac{{\rm d}\langle\Delta \boldsymbol{L}\rangle}{{\rm d}t} = -n\sqrt{\frac{mkT}{2\pi}} \oint {\rm d}S\, (\boldsymbol{r}\times\hat{\boldsymbol{n}})(\boldsymbol{v}_0\cdot\hat{\boldsymbol{n}}). \quad (119)$$

Substituting $\boldsymbol{v}_0 = \boldsymbol{\Omega}\times\boldsymbol{r}$, we conclude that

$$\frac{{\rm d}\langle\Delta \boldsymbol{L}\rangle}{{\rm d}t} = -n\sqrt{\frac{mkT}{2\pi}} \oint {\rm d}S\, (\boldsymbol{r}\times\hat{\boldsymbol{n}})[(\boldsymbol{r}\times\hat{\boldsymbol{n}})\cdot\boldsymbol{\omega}]. \quad (120)$$

The triple product implies that this zero if $\boldsymbol{\omega}$, $\boldsymbol{r}$ and $\hat{\boldsymbol{n}}$ are coplanar, which is the case for grains rotating around an axis of symmetry. In our case, however, it is non-zero. We note that the average value of the dyadic $(\boldsymbol{r}\times\hat{\boldsymbol{n}})(\boldsymbol{r}\times\hat{\boldsymbol{n}})$ over a disc is $\frac{1}{4}R^2(\hat{\boldsymbol{i}}\hat{\boldsymbol{i}} + \hat{\boldsymbol{j}}\hat{\boldsymbol{j}})$, where R is the disc radius and $\hat{\boldsymbol{i}}\hat{\boldsymbol{i}} + \hat{\boldsymbol{j}}\hat{\boldsymbol{j}}$ is the projector into the plane of the grain. Therefore,

$$\frac{{\rm d}\langle\Delta \boldsymbol{L}\rangle}{{\rm d}t} = -n\sqrt{\frac{mkT}{2\pi}}\,\frac{1}{4}R^2 S\boldsymbol{\omega}_{\rm ip}, \quad (121)$$

where $\boldsymbol{\omega}_{\rm ip}$ is the in-plane part of the instantaneous angular velocity. It is equal to $\boldsymbol{\omega}_{\rm ip} = \boldsymbol{L}_{\rm ip}/I_1$. Further using $I_1 = \frac{1}{2}I_3$, we find

$$\frac{{\rm d}\langle\Delta \boldsymbol{L}\rangle}{{\rm d}t} = -n\sqrt{\frac{mkT}{2\pi}}\,\frac{\pi R^4}{I_3}\boldsymbol{L}_{\rm ip} = -\frac{n}{n_{\rm H}}\sqrt{\frac{m}{m_{\rm H}}}\,\tau_{\rm H}^{-1}\boldsymbol{L}_{\rm ip}, \quad (122)$$

where we have used the definition of $\tau_{\rm H}$ and $a_{\rm cx}^4 \equiv \frac{3}{8}R^4$ in the last line.[17]

In order to complete the derivation, we need the mean value of $\boldsymbol{L}_{\rm ip}$ over nutation angles and time. We note that this mean value must be in the direction of $\boldsymbol{L}$, and that

$$\boldsymbol{L}_{\rm ip}\cdot\boldsymbol{L} = L_{\rm ip}^2 = L^2\sin^2\theta, \quad (123)$$

which has mean value $\frac{2}{3}L^2$. Therefore the mean value of $\boldsymbol{L}_{\rm ip}$ is $\frac{2}{3}\boldsymbol{L}$ and we find

$$F_{\rm n}^{\rm (in)} = \frac{2}{3}\frac{n}{n_{\rm H}}\sqrt{\frac{m}{m_{\rm H}}}. \quad (124)$$

The total drag coefficient is the sum,

$$F_{\rm n} = F_{\rm n}^{\rm (in)} + F_{\rm n}^{\rm (ev)} = \frac{5}{3}\frac{n}{n_{\rm H}}\sqrt{\frac{m}{m_{\rm H}}}. \quad (125)$$

[16] The + sign for this term arises because for $\boldsymbol{v}_0\cdot\hat{\boldsymbol{n}} > 0$, $\mathcal{H}^{\rm c}$ expands.

[17] The excitation radius $a_{\rm cx}$ is the same as in AHD09 when taking the limit of infinitesimally thin discs (AHD09 assumed discs with a thickness $d = 3.35$ Å).

7.2 Excitation rate: neutral grains, neutral impactors

We now consider the stochastic change in angular momentum due to collisions with incoming particles. This excitation rate (unlike the damping rate) can be computed at zero grain rotation. The impact of a particle with velocity $\boldsymbol{v}$ at position $\boldsymbol{r}$ imparts an angular momentum $\Delta\boldsymbol{L} = m\,\boldsymbol{r}\times\boldsymbol{v}$. The stochastic change in angular momentum along the z-axis can be written as:

$$\frac{{\rm d}\langle\Delta L_z^2\rangle}{{\rm d}t} = m^2 \oint {\rm d}S \int_{\mathcal{H}^{\rm c}} {\rm d}^3\boldsymbol{v}\, [\hat{\boldsymbol{z}}\cdot(\boldsymbol{r}\times\boldsymbol{v})]^2(-\boldsymbol{v}\cdot\hat{\boldsymbol{n}})\, f(\boldsymbol{r},\boldsymbol{v}). \quad (126)$$

The triple product can be cyclically permuted to get

$$\frac{{\rm d}\langle\Delta L_z^2\rangle}{{\rm d}t} = -m^2 \oint {\rm d}S \int_{\mathcal{H}^{\rm c}} {\rm d}^3\boldsymbol{v}\, (\boldsymbol{v}\cdot\boldsymbol{q})^2(\boldsymbol{v}\cdot\hat{\boldsymbol{n}})\, f(\boldsymbol{r},\boldsymbol{v}), \quad (127)$$

where $\boldsymbol{q} \equiv \hat{\boldsymbol{z}}\times\boldsymbol{r}$. The integration over velocity is a Gaussian times a cubic polynomial over a half-space, which evaluates to

$$-\frac{1}{\sqrt{2\pi}}\, n \left(\frac{kT}{m}\right)^{3/2} [\, q^2 + (\boldsymbol{q}\cdot\hat{\boldsymbol{n}})^2\,], \quad (128)$$

so

$$\frac{{\rm d}\langle\Delta L_z^2\rangle}{{\rm d}t} = \sqrt{\frac{m(kT)^3}{2\pi}}\, n \oint {\rm d}S\, [\, q^2 + (\boldsymbol{q}\cdot\hat{\boldsymbol{n}})^2\,]. \quad (129)$$

Now the integrand is a scalar and hence may be evaluated in either inertial or grain-fixed coordinates. We choose the grain-fixed coordinates. The nutation angle average is then equivalent to averaging over the direction of $\hat{\boldsymbol{z}}$, which leads to the dyadic relation

$$\langle\boldsymbol{q}\boldsymbol{q}\rangle = \frac{1}{3}(r^2\boldsymbol{1} - \boldsymbol{r}\boldsymbol{r}), \quad (130)$$

where $\boldsymbol{1}$ is the unit dyadic. This implies that

$$\langle q^2 + (\boldsymbol{q}\cdot\hat{\boldsymbol{n}})^2\rangle = r^2 - \frac{1}{3}(\boldsymbol{r}\cdot\hat{\boldsymbol{n}})^2. \quad (131)$$

Plugging into equation (129) and converting to the G-factor gives

$$G_{\rm n}^{\rm (in)} = \frac{n}{n_{\rm H}}\sqrt{\frac{m}{m_{\rm H}}}\,\frac{3}{16\pi a_{\rm cx}^4} \oint {\rm d}S[r^2 - \frac{1}{3}(\boldsymbol{r}\cdot\hat{\boldsymbol{n}})^2]. \quad (132)$$

For a disc, the integral is $\pi\, R^4$ and $a_{\rm cx}^4 = \frac{3}{8}R^4$, so it follows that

$$G_{\rm n}^{\rm (in)} = \frac{1}{2}\frac{n}{n_{\rm H}}\sqrt{\frac{m}{m_{\rm H}}}. \quad (133)$$

Thus, the collisional excitation rate for incoming particles is the same as it is for the case of the grain rotating around a principal axis of inertia.

The calculation for evaporating particles is the same except that we replace $T \to T_{\rm ev}$:

$$G_{\rm n}^{\rm (ev)} = \frac{1}{2}\frac{n}{n_{\rm H}}\sqrt{\frac{m}{m_{\rm H}}}\,\frac{T_{\rm ev}}{T}. \quad (134)$$

Once again, there is no difference from the case of rotation around I_3.

7.3 Excitation and damping: charged grain, neutral impactor

The case of a charged grain is different from a neutral grain because of the induced dipole attraction between the grain and the atom. The interaction potential is given by

$$V(r) = -\frac{1}{2}\alpha\frac{Z_g^2 q_e^2}{r^4}. \quad (135)$$

We can solve for the critical separation r_c at which the induced dipole attraction overwhelms the thermal energy of the gas, i.e. where $V(r_c) = \frac{3}{2}kT$:

$$r_c = \sqrt[4]{\frac{Z_g^2 q_e^2 \alpha}{3kT}} \approx 1.5 \left(\frac{\alpha Z_g^2}{0.67\text{Å}^3}\right)^{1/4} \left(\frac{T}{8000\ \text{K}}\right)^{-1/4} \text{Å}. \quad (136)$$

In the cases where $r_c \ll a_{cx}$, the induced dipole attraction is a small perturbation and the coefficients $F_n^{(in)}$, $G_n^{(in)}$, $F_n^{(ev)}$ and $G_n^{(ev)}$ are unchanged from the case of a neutral grain. On the other hand, if $r_c \gg a_{cx}$, then an incoming particle is certain to impact the grain surface if it passes over the barrier in the effective potential $V_{err}(r) = L_n^2/mr^2 + V(r)$, irrespective of the details of the asymmetry of the grain (a disc-like grain has a quadrupole moment, but at $r \gg a_{cx}$ the potential is dominated by the monopole charge). Therefore, in this alternative case, the shape of the grain is irrelevant, and we should use the AHD09 values for the coefficients $F_n^{(in)}$ and $G_n^{(in)}$.

While $G_n^{(in)}$ is the same in both of our limiting cases ($r_c/a_{cx} \gg 1$ or $\ll 1$), $F_n^{(in)}$ is not the same and it is necessary to interpolate between the two solutions. We must have $F_n^{(in)}/F_n \to 0$ for $r_c/a_{cx} \gg 1$ and $F_n^{(in)} \to \frac{2}{3}F_{n,AHD09}$ for $r_c/a_{cx} \ll 1$. A simple heuristic interpolating function[18] is

$$F_n^{(in)} = \frac{2}{3}F_{n,AHD09}\left[1 + \left(\frac{r_c}{a_{cx}}\right)^2\right]^{-1}. \quad (137)$$

In diffuse phases of the ISM, collisions with neutral impactors are in general not the dominant rotational damping mechanism (see e.g. fig. 4 of DL98b). The exact shape of the interpolation function is therefore irrelevant in these cases. In very specific environments though, for example in extremely dense PDRs, and for low enough values of the dipole moment, collisions of neutral impactors on charged grains may dominate the rotational damping. If this is the case, one should be aware that F_n is uncertain in the region $r_c \sim a_{cx}$ and that this uncertainty will propagate on the resulting spectrum, as $\nu_{peak} \propto \sqrt{G/F_n}$ and $j_{tot} \propto (G/F_n)^2$.

For the evaluation of damping and excitation due to evaporating particles, there is no such ambiguity over which case to take since we found that the excitation is the same for both the uniform $\theta = 0$ rotation (old case) and isotropic θ distribution (new case).

7.4 Excitation and damping: neutral grain, charged impactor

We now consider the case of an ion impacting a neutral grain. The analysis of evaporating particles is the same as that treated in Sections 7.1 and 7.2, since the ion is assumed to recombine on the grain surface and evaporate as a neutral.

Incoming ions follow a trajectory influenced by the dipole moment of the grain, both permanent and induced. The characteristic induced dipole energy for a grain with radius R is $E_{id} \sim q_e^2 R^{-1}$ (i.e. the attraction of the ion to the mirror charge). For the PAH sequence, $R \approx 0.9 N_C^{1/2}$ Å, so we find $E_{id}/k = 1.7 \times 10^5 N_C^{-1/2}$ K. Thus even at $N_C \approx 100$ (our largest disc-like grains), the induced dipole energy is well above the temperature of the gas even in warm phases (WNM, WIM). Therefore to a first approximation, we treat the probability of an incoming ion striking the grain surface as being determined by the dipole interactions rather than grain geometry. (Since the polarizability tensor of the grain is not isotropic, this is only an approximation.) In this case, we are justified in using the AHD09 rates for incoming particles. We are thus led to the conclusion that the AHD09 rates are applicable to ion impacts on neutral grains, both for the incoming coefficients F, $G_i^{(in)}$ and as previously described for the evaporation coefficients F, $G_i^{(ev)}$.

[18] Since $F_{n,AHD09} \propto (\frac{r_c}{a_{cx}})^4$ for $r_c \gg a_{cx}$, our heuristic prescription for $F_n^{(in)}$ is such that $F_n^{(in)} \nrightarrow 0$ in that limit. It is not clear whether $F_n^{(in)}$ should tend to zero for $r_c \gg a_{cx}$, since although the relative difference in collisional rates between impactors on prograde orbits and retrograde orbits should vanish, the overall collision rate increases because of electrostatic focusing. However, only the relative contribution $F_n^{(in)}/F_n$ matters so this should not be a concern.

7.5 Excitation and damping: charged grain, charged impactor

In the case of an ion colliding with a charged grain, the particles interact with the Coulomb potential, which has magnitude

$$V(r) = \frac{q_e^2}{r} \quad (138)$$

for single charges (and more for multiple charges). A simple calculation then shows that for practical cases with the grains that are treated as disc-like ($a < 6$ Å), ISM temperatures in most phases of interest (including warm phases) will have $\frac{3}{2}kT \ll q_e^2/a$. In this case, the angular momentum transferred to the grain by incoming particles is geometry-independent: positive grains will receive essentially no impacts, while negative grains will be impacted by (and acquire the angular momentum of) any particle that passes close enough to the grain. Thus, the incoming rates F, $G_i^{(in)}$ are left unaffected. The outgoing rates F, $G_i^{(ev)}$ are also unaffected: since the particles are neutral when they evaporate off the grain, the outgoing rates are as computed in the previous section.

7.6 Summary

We may now summarize the key differences between our investigation and that of AHD09.

For the case of neutral grains and neutral impactors, we have thus found the coefficients:

$$F_n = \frac{5}{3}F_{n,AHD09} \text{ and } G_n = G_{n,AHD09}. \quad (139)$$

For charged grains and neutral impactors,

$$F_n^{(in)} = \left\{1 + \frac{2}{3}\left[1 + \left(\frac{r_c}{a_{cx}}\right)^2\right]^{-1}\right\} F_{n,AHD09} \quad (140)$$

and

$$G_n = G_{n,AHD09}. \quad (141)$$

The case of ion impacts is left unchanged from AHD09.

8 RESULTS

To avoid lengthy repetitions, we will refer to the case where grains are spinning around their axis of greatest inertia (as treated by DL98b and AHD09) by 'case 1', and to the case where the relative orientation of the grain and the angular momentum is randomized (as discussed in the present work) by 'case 2'.

8.1 Angular momentum distribution

We saw in Section 4.1 that, at equal angular momentum, the total power radiated by a disc-like grain in case 2 was five times (in the

case $\mu_{\rm op}=0$) to ∼10 times ($\mu_{\rm ip}^2:\mu_{\rm op}^2=2:1$) higher than the power radiated in case 1. This ratio goes even higher as one increases the $\mu_{\rm op}^2:\mu_{\rm ip}^2$ ratio. However, the angular momentum distribution is different in each case, and, as $P\propto L^4$, the ratio of the total power emitted will really be

$$\frac{P_{\rm case2}}{P_{\rm case1}}\approx 10\frac{\langle L^2\rangle_{\rm case2}^2}{\langle L^2\rangle_{\rm case1}^2}. \tag{142}$$

In what follows we show that $\langle L^2\rangle_{\rm case2}<\langle L^2\rangle_{\rm case1}$.

First of all, we showed in earlier sections that the damping rates are generally higher for grains spinning around a non-principal axis. This can be understood heuristically as follows: for a given angular momentum L, the rotational energy $E_{\rm rot}(L,\theta)$ as a function of the nutation angle was given in equation (3). Averaging over angles, we find that

$$\langle E_{\rm rot}\rangle(L)=\frac{L^2}{2I_1}-\frac{1}{3}\frac{L^2}{2}\left(I_1^{-1}-I_3^{-1}\right). \tag{143}$$

In the case of a disc-like grain ($I_3=2I_1$) this is

$$\langle E_{\rm rot}\rangle(L)=\frac{5}{3}\frac{L^2}{2I_3}=\frac{5}{3}E_{\rm rot}(L,\theta=0). \tag{144}$$

Therefore, we may expect that, when in contact with a bath of a characteristic energy, grains with a randomly oriented rotation axis will have an rms angular momentum $\sim\sqrt{5/3}$ times smaller than those rotating around the axis of greatest inertia. This is indeed what we found in the case of collisions of neutral grains with neutral impactors, or emission of infrared photons, for which we showed that G was unchanged but F was increased by a factor of 5/3. We also showed that the normalized plasma damping and excitation rates satisfied $1<F_{\rm p}/G_{\rm p}<3$.

More importantly, the characteristic radiation–reaction damping time $\tau_{\rm ed}$ was found to be shorter in case 2. We have

$$\frac{\tau_{\rm ed}(\theta\ {\rm random})}{\tau_{\rm ed}(\theta=0)}=\frac{\mu_{\rm ip}^2}{\frac{41}{15}\mu_{\rm ip}^2+\frac{16}{3}\mu_{\rm op}^2}. \tag{145}$$

In the case where radiation–reaction is the dominant rotational damping mechanism, which is the case for the smallest grains in diffuse phases of the ISM, AHD09 showed that the rms angular momentum is $\propto\tau_{\rm ed}^{1/4}$. Numerically, we have

$$\frac{\tau_{\rm ed}^{1/4}(\theta\ {\rm random})}{\tau_{\rm ed}^{1/4}(\theta=0)}\approx\begin{cases}0.78 & \mu_{\rm op}=0,\\ 0.66 & \mu_{\rm ip}^2:\mu_{\rm op}^2=2:1.\end{cases} \tag{146}$$

From these considerations, we therefore expect that in the same environment, the characteristic angular momentum in case 2 will be ∼0.66–0.78 times the one in case 1.

We show in Fig. 3 the angular momentum distribution for a grain of volume-equivalent radius $a=5$ Å, in WIM conditions, with $\mu_{\rm ip}^2:\mu_{\rm op}^2=2:1$, and with dipole moment per atom $\beta=0.38$ debye. The rms angular momentum in case 2 is ∼0.67 times the one in case 1.

8.2 Change in emissivity

At a given angular momentum, the power radiated in case 2 peaks at a frequency approximately twice higher than the power radiated in case 1 (see discussion in Section 4.1).

Therefore, and in view of the preceding section, we expect that the total power radiated in case 2 will peak at a frequency $\sim2\times0.7\sim1.4$ times higher and will integrate to a total power $\sim10\times(0.7)^4\sim2$ times the power radiated in case 1. This is indeed what we find, as can be seen in Fig. 4.

The overall spinning dust emissivity follows the same trends, as can be seen in Fig. 5 for the WIM, and in Fig. 6 for other interstellar environments.

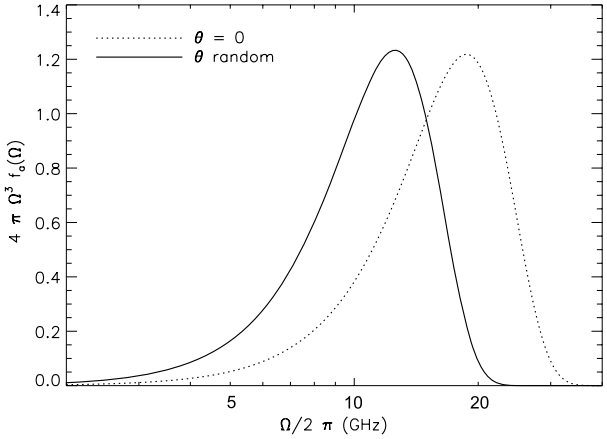

Figure 3. Probability distribution function for the parameter $\Omega=L/I_3$, for a grain of radius $a=5$ Å, in WIM conditions, with $\mu_{\rm ip}^2$:$\mu_{\rm op}^2=2$:1, and with dipole moment per atom $\beta=0.38$ debye.

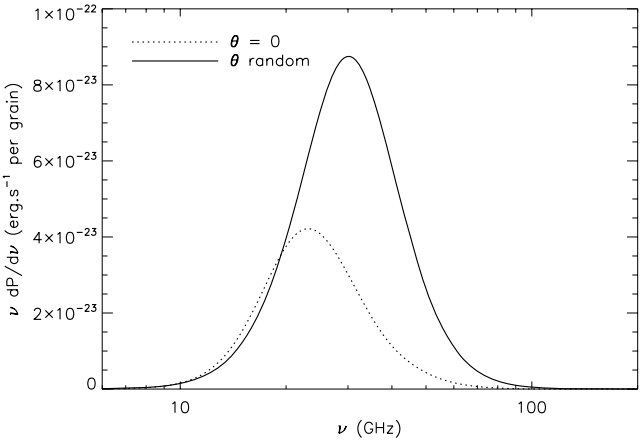

Figure 4. Power radiated by a grain of radius $a=5$ Å, in WIM conditions, with $\mu_{\rm ip}^2$:$\mu_{\rm op}^2=2$:1, and with dipole moment per atom $\beta=0.38$ debye.

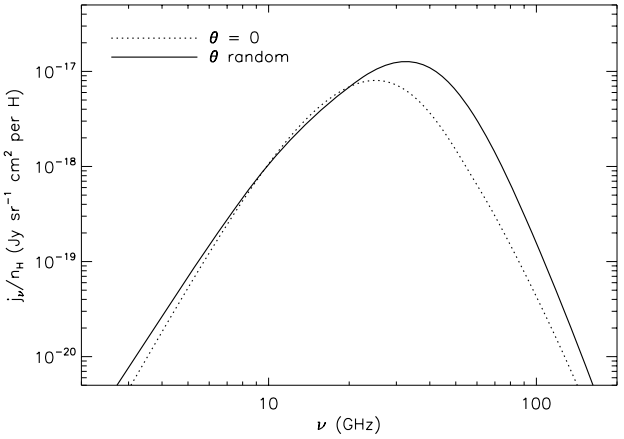

Figure 5. Spinning dust emissivity in WIM environment.

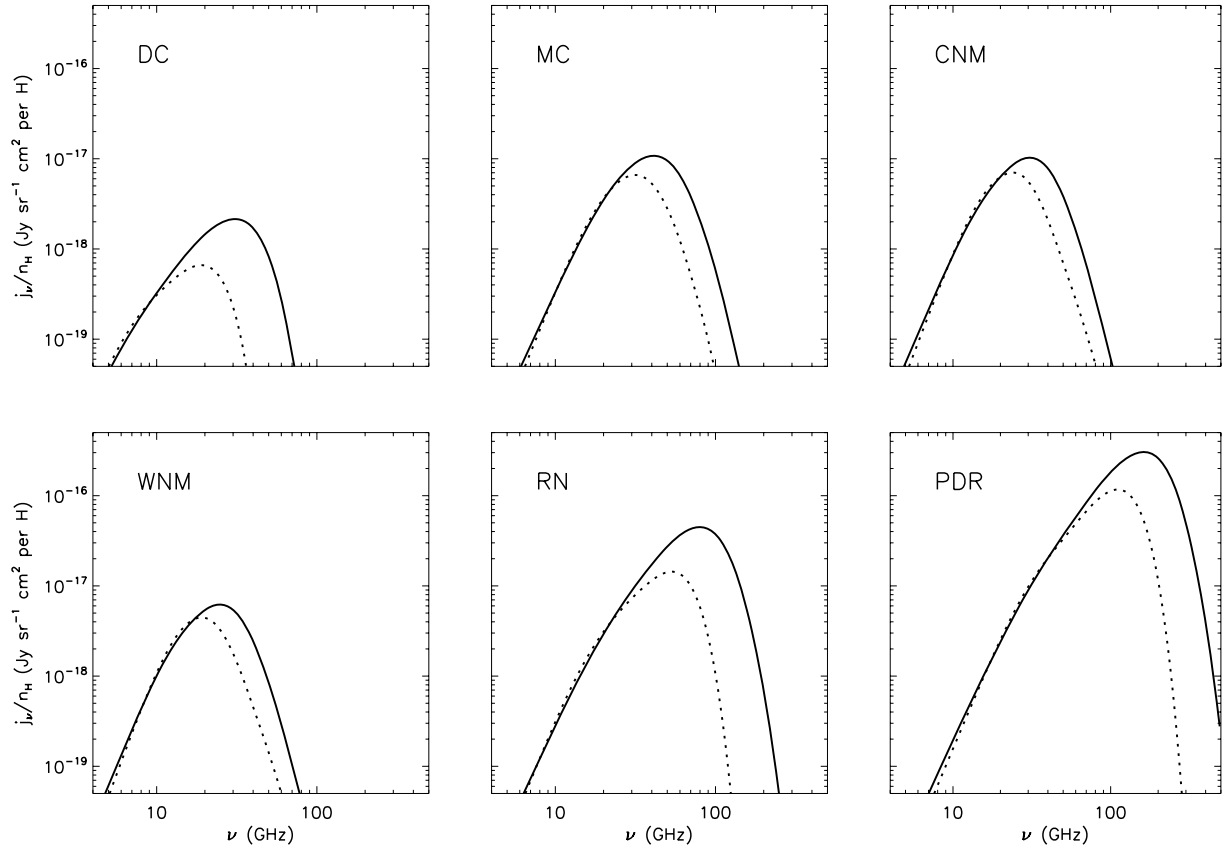

Figure 6. Spinning dust spectra for several environmental conditions: (DC), MC, CNM, WNM, RN and PDR. The environments are defined in DL98b, table 1. The parameters for the grain size distribution are $R_V = 3.1, b_C = 6 \times 10^{-5}$ for the diffuse CNM and WNM phases, and $R_V = 5.5, b_C = 3 \times 10^{-5}$ for the dense DC, MC, RN and PDR. The dashed line is for a spectrum calculated assuming case 1 ($\theta = 0$), whereas the solid line is for case 2 (isotropic θ). The shift to higher frequencies and increase in emissivity in case 2 are systematic for all environments. We expect that case 2 should be a better approximation in the diffuse and high radiation intensity phases (WIM, CNM, WNM, RN, PDR).

8.3 Sensitivity to dipole moment orientation

It is not clear what is the correct assignment for the direction of the grain permanent dipole moment relative to the principal axes. Here, we analyse the effect of the dipole moment orientation on the spinning dust spectrum; it appears to make only a minor difference in the WIM environment.

For the smallest grains where radiation–reaction damping is most important, we expect $\langle\Omega^2\rangle^{1/2} \propto \tau_{\rm ed}^{1/4}$ so

$$\langle\Omega^2\rangle^{1/2} \propto \begin{cases} \mu_{\rm ip}^{-1/2} & \text{(case 1)}, \\ \mu^{-1/2}\left(\dfrac{80}{39} - \dfrac{\mu_{\rm ip}^2}{\mu^2}\right)^{-1/4} & \text{(case 2)}. \end{cases} \quad (147)$$

In case 1, the rotation rate is very sensitive to the orientation of the dipole moment (only the in-plane component contributes to the power and the radiation reaction damping). Eventually, when the in-plane component becomes small enough, radiation–reaction damping becomes subdominant and the rms angular momentum will depend only on interactions with gas or infrared photons. In case 2, however, the dependence on $\mu_{\rm ip}^2/\mu^2$ is quite weak, as the out-of-plane component contributes to the power and angular momentum loss. We show the normalized rms angular momenta in case 1 and 2 in Fig. 7. Fig. 7 also shows an estimate of the peak frequency of the emitted power in both cases.

The total power radiated by one grain, at a given angular momentum, was given in equation (40) for case 2. Taking $\Omega \sim \langle\Omega^2\rangle^{1/2}$, and using the above results, we obtain

$$P \propto \begin{cases} \text{constant} & \text{(case 1)} \\ \left(\frac{32}{17} - \frac{\mu_{\rm ip}^2}{\mu^2}\right) \Big/ \left(\frac{80}{39} - \frac{\mu_{\rm ip}^2}{\mu^2}\right) & \text{(case 2)}. \end{cases} \quad (148)$$

Thus in both cases the total power is very nearly independent of $\mu_{\rm ip}^2/\mu^2$. In case 1, when $\mu_{\rm ip}^2/\mu^2 \to 0$, radiation–reaction damping becomes subdominant and the power becomes proportional to $\mu_{\rm ip}^2$. These features are shown in Fig. 8.

9 DISCUSSION

The purpose of this work was to revisit the assumption of DL98b and AHD09 that PAHs rotate about their axis of main inertia. The motivation in doing so is that thermal spikes following the absorption of UV photons randomize the orientation of the grain with respect to the angular momentum axis. These absorption events happen frequently enough (i.e. on time-scale shorter than the time-scale for significant changes in the total angular momentum) that we expect such a randomization to be effective in most environments. Thus, we expect the results from this work ('case 2') to be a better approximation to diffuse or high-radiation environments (CNM, WNM, WIM, PDR and RN) than those from AHD09, which assumed rapid dissipation of the nutational energy ($\theta = 0$ or 'case 1'). However, the new release of SpDust allows the user to choose either case; for example, one may wish to explore the range of cases in dark cloud (DC) environments where thermal spikes are infrequent, or what

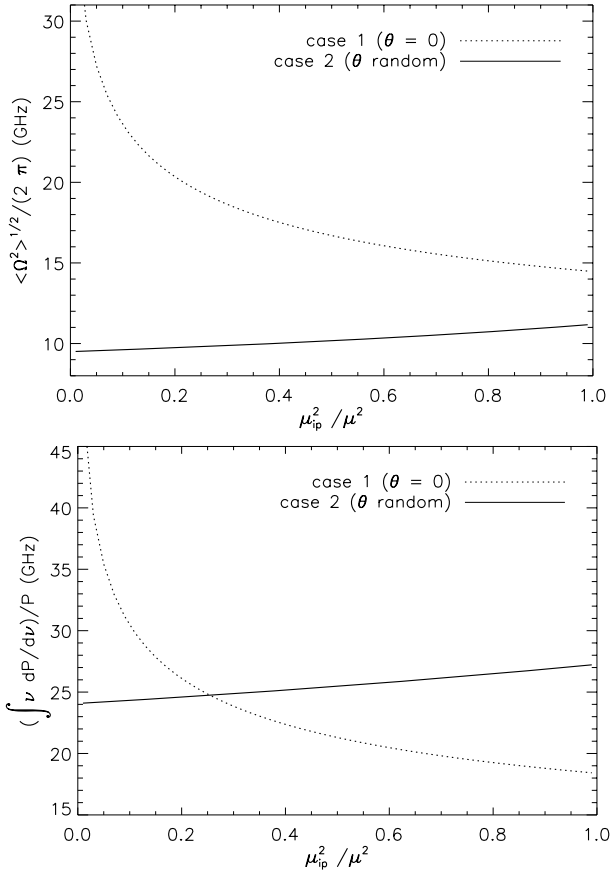

Figure 7. Top panel: normalized rms angular momentum $\langle\Omega^2\rangle^{1/2}$ as a function of the ratio of in-plane to total dipole moment. Bottom panel: estimate of the peak frequency $\int \nu(\mathrm{d}P/\mathrm{d}\nu)\mathrm{d}\nu/P$, as a function of this ratio. Both are for a dust grain of radius $a = 5$ Å and dipole moment per atom $\beta = 0.38$ debye, in WIM conditions.

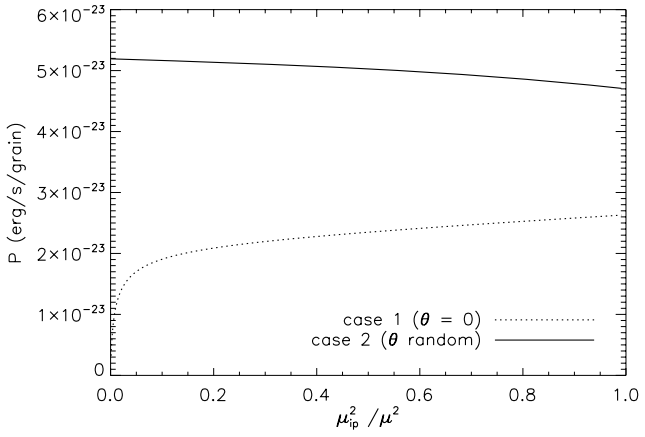

Figure 8. Total power emitted by a dust grain of radius $a = 5$ Å and dipole moment per atom $\beta = 0.38$ debye, in WIM conditions, as a function of the ratio of in-plane to total dipole moment.

happens if an as-yet-unidentified dissipational process is active and restores $\theta = 0$.

In this work, we showed that, for a given angular momentum, the power radiated by a grain in case 2 is ∼10 times higher than that radiated by a grain in case 1. This is because in case 2, the grain emits at higher frequencies, including above the one corresponding to the instantaneous angular velocity, as it is not rotating around the axis of greatest inertia.

We evaluated the rotational excitation and damping rates in case 2 as a function of grain size and environment conditions, and the resulting angular momentum distribution. We showed that in a given environment, grains in case 2 have a lower rms angular momentum than those in case 1, by a factor of ∼0.7. This is due to larger damping rates, in particular radiation–reaction damping, in case 2.

The combination of these results leads to a spinning dust spectrum peaking at slightly higher frequencies in case 2, and a total power approximately twice as large as that emitted in case 1. Finally, we showed that the spectrum in case 2 is only weakly sensitive to the precise value of the $\mu_{\rm ip}^2 : \mu_{\rm op}^2$ ratio.

Dobler et al. (2009) found a tension between theoretical results and microwave observations of the WIM: the theory was a factor of ∼3 larger than the observations, and the peak frequency of the spinning dust and its amplitude could not be simultaneously reconciled by changing β (the normalization of the dipole moment). By increasing the theoretical emissivity and moving its peak to higher frequencies, our results may worsen this tension. This seems likely to strengthen the empirical case for depletion of the PAH population in the WIM phase, however there are other conceivable explanations for this discrepancy. The random walk model for the dipole moment may not apply well to the smallest grains (e.g. one could imagine that some of the small PAHs have symmetries that guarantee $\boldsymbol{\mu} = 0$ exactly), or one could imagine extra low-frequency internal degrees of freedom which allow the grain to relax to a state where it rotates around the axis of greatest moment of inertia. A detailed exploration of the parameter space (as was done by Dobler et al. 2009) is beyond the scope of this paper.

As a final note, we present some of the remaining issues in the treatment of the rotational physics of the smallest dust grains.

(i) *Triaxiality*: many PAHs have triaxial moment of inertia tensors (e.g. ovalene $C_{32}H_{14}$, circumpyrene $C_{42}H_{16}$ and their derivatives). This case was not treated in the present paper due to its much greater complexity: since the dipole moment then depends on elliptic functions of the angle conjugate to the nutation action, a countably infinite number of frequencies are emitted. Aside from this aspect, however, the underlying formalism in this paper would be applicable: the nutation action (rather than $hK = 2\pi L\cos\theta$) would be conserved in free rotation and we would average over this action instead of $\cos\theta$. The analysis would also break into two cases depending on whether the grain lies on the short-axis or long-axis side of the separatrix.

(ii) *Impulsive torques*: some of the sources of torque, such as ion impacts, impart large but infrequent changes in angular momentum. This could in principle lead to 'rotational spikes' analogous to the well-known thermal spikes in the grains' internal energy, and would not be treated correctly by the Fokker–Planck equation (which is a diffusive approximation).[19]

(iii) *Ancillary data*: we have not fully quantified the uncertainties in the ancillary data, such as evaporation temperatures, the emissivity in the lowest-frequency vibrational modes and the grain charging model (photoelectric and electron/ion impact). However, our hope in making the SPDUST code publicly available is to provide users the flexibility to explore deviations from default or fiducial parameters.

[19] This issue is treated in Hoang et al. (2010); they find that the principal effect on the spinning dust spectrum is the existence of a 'tail' to high frequencies resulting from transient spin-up of the grains.

ACKNOWLEDGMENTS

We thank Bruce Draine and Nathalie Ysard for numerous conversations about the physics of grain rotation, and Clive Dickinson for reading the manuscript and testing SPDUST v2.0.

KS would like to thank Edward C. and Alice Stone for their support for the Summer Undergraduate Research Fellowship programme at Caltech. YA-H and CH are supported by the US Department of Energy (DE-FG03-92-ER40701) and the National Science Foundation (AST-0807337). CH is supported by the Alfred P. Sloan Foundation.

REFERENCES

Ali-Haïmoud Y., Hirata C., Dickinson C., 2009, MNRAS, 395, 1055 (AHD09)
Anderson N., Watson W., 1993, A&A, 270, 477
Bennett C. et al., 2003, ApJS, 148, 97
Casassus S., Cabrera G., Förster F., Pearson T., Readhead A., Dickinson C., 2006, ApJ, 639, 951
Casassus S., Nyman L., Dickinson C., Pearson T., 2007, MNRAS, 382, 1607
Casassus S. et al., 2008, MNRAS, 391, 1075
Davies R., Dickinson C., Banday A. J., Jaffe T. R., Gorski K. M., Davis R. J., 2006, MNRAS, 370, 1125
de Oliveira-Costa A., Kogut A., Devlin M. J., Netterfield C. B., Page L. A., Wollack E. J., 1997, ApJ, 482, L17
de Oliveira-Costa A., Tegmark M., Gutiérrez C. M., Aled W., Davies R. D., Lasenby A. N., Rebolo R., Watson R. A., 1999, ApJ, 527, L9
Dickinson C., Davis R. D., Bronfman L., Casassus S., Davis R. J., Pearson T. S., Readhead A. C. S., Wilkinson P. N., 2007, MNRAS, 379, 297
Dickinson C. et al., 2009, ApJ, 690, 1585
Dobler G., Finkbeiner D., 2008, ApJ, 680, 1235
Dobler G., Draine B., Finkbeiner D., 2009, ApJ, 699, 1374
Draine B., Lazarian A., 1998a, ApJ, 494, L19
Draine B., Lazarian A., 1998b, ApJ, 508, 157 (DL98b)
Draine B., Lazarian A., 1999, ApJ, 512, 740
Draine B., Li A., 2001, ApJ, 551, 807
Draine B., Sutin B., 1987, ApJ, 320, 803
Erickson W., 1957, ApJ, 126, 480
Ferrara A., Dettmar R.-J., 1994, ApJ, 427, 155
Finkbeiner D., 2003, ApJS, 146, 407
Finkbeiner D., 2004, ApJ, 614, 186
Finkbeiner D., Davis M., Schlegel D., 1999, ApJ, 524, 867
Finkbeiner D., Langston G., Minter A., 2004, ApJ, 617, 350
Fraisse A., Brown J., Dobler G. et al., 2009, in Dodelson S. et al., eds., AIP Conf. Ser. Vol. 1141, CMB Polarization Workshop: Theory and Foregrounds. AIP, Melville, NY, p. 265
Gold B. et al., 2009, ApJS, 180, 265
Hand L., Finch J., 1998, Analytical Mechanics. Cambridge University Press, Cambridge, UK
Haslam C., Salter C., Stoffel H., Wilson W., 1982, A&AS, 47, 1
Hedberg L., Hedberg K., Cheng P., Scott L., 2000, J. Phys. Chem. A, 104, 7689
Hoang T., Draine B., Lazarian A., 2010, ApJ, 715, 1462
Hoyle F., Wickramasinghe C., 1970, Nat, 227, 473
Hudgins D., Bauschlicher C., Allamandola L., 2005, ApJ, 632, 316
Jones R., Spitzer L., 1967, ApJ, 147, 943
Kogut A., Banday A. J., Bennett C. L., Gorski K. M., Hinshaw G., Reach W. T., 1996a, ApJ, 460, 1
Kogut A., Banday A. J., Bennett C. L., Gorski K. M., Hinshaw G., Smoot G. F., Wright E. I., 1996b, ApJ, 464, L5
Kroto H., 1992, Molecular Rotation Spectra. Dover Publications, Inc., Mineola, NY
Lazarian A., Roberge W., 1997, ApJ, 484, 230
Leger A., 1988, in Coyne G., Magalhaes A. M., Moffat A. F., Schulte-Ledbeck R. E., Tapia S., eds., Polarized Radiation of Circumstellar Origin. University of Arizona Press, Tucson, AZ, p. 769
Leitch E., Readhead A., Pearson T., Myers S., 1997, ApJ, 486, L23
Le Page V., Snow T., Bierbaum V., 2003, ApJ, 584, 316
Li A., Draine B., 2001, ApJ, 554, 778
Mathis J., Mezger P., Panagia N., 1983, A&A, 128, 212
Mezger P., Mathis J., Panagia N., 1982, A&A, 105, 372
Murphy E. et al., 2010, ApJ, 709, L108
Page L. et al., 2007, ApJS, 170, 335
Pilleri P. et al., 2009, MNRAS, 397, 1053
Purcell E., 1979, ApJ, 231, 404
Ragot B., 2002, ApJ, 568, 232
Rouan D., Léger A., Omont A., Giard M., 1992, A&A, 253, 498
Scaife A. et al., 2007, MNRAS, 377, L69
Sironi L., Draine B., 2009, ApJ, 698, 1292
Tegmark M., Eisenstein D., Hu W., de Oliveira-Costa A., 2000, ApJ, 530, 133
Watson R. A., Rebolo R., Rubíño-Martin J. A., Hildebrandt S., Gutiérrez C. M., Fernández-Cerezo S., Hoyland R. J., Batistelli E. S., 2005, ApJ, 624, L89
Weingartner J., Draine B., 2001a, ApJS, 134, 263
Weingartner J., Draine B., 2001b, ApJ, 548, 296
Ysard N., Verstraete L., 2010, A&A, 509, 12

APPENDIX A: IMPLEMENTATION OF PLASMA DRAG INTEGRALS

Here, we describe our implementation of the plasma drag coefficients, equations (91) and (93), in SpDust. These are integrals over the $G_{\rm p,AHD}(\omega)$ function, which is itself time-consuming to compute.

If we wish to calculate the integral $\int w(x)g(x)\mathrm{d}x$, where $w(x)$ is a known weighing function, properties of which will be discussed later, and the function $g(x)$ is smooth enough on the interval of integration that it can be approximated by a quadratic polynomial $g(x) \approx a + bx + cx^2$, then we may approximate

$$\int w(x)g(x)\mathrm{d}x \approx A\left[g(x_+) + g(x_-)\right], \tag{A1}$$

where $A \equiv \frac{1}{2}\int w(x)\mathrm{d}x$, and $\{x_+, x_-\}$ are the solutions of the second-order system

$$\begin{cases} x_+ + x_- = A^{-1}\int x w(x)\mathrm{d}x, \\ x_+^2 + x_-^2 = A^{-1}\int x^2 w(x)\mathrm{d}x. \end{cases} \tag{A2}$$

We now turn our attention to the specific cases of $G_{\rm p}(\Omega)$ and $F_{\rm p}(\Omega)$. With $x = \omega/\Omega$ and the weighing function $w(x) = (3-x)^2$, we get

$$G_{\rm p}(\Omega) \approx \frac{2\mu_{\rm op}^2}{3\mu_{\rm ip}^2} G_{\rm p,AHD}(2\Omega) + \frac{1}{3}\left[G_{\rm p,AHD}(\Omega_+) + G_{\rm p,AHD}(\Omega_-)\right], \tag{A3}$$

where

$$\Omega_\pm = \frac{3 \pm \sqrt{3/5}}{2}\Omega \approx \{1.11\Omega, 1.89\Omega\}. \tag{A4}$$

Similarly, with the weighing function $w(x) = x(3-x)^2$, we get

$$F_{\rm p}(\Omega) \approx \frac{4\mu_{\rm op}^2}{3\mu_{\rm ip}^2} G_{\rm p,AHD}(2\Omega) \tag{A5}$$

$$+\frac{1}{2}\left[G_{\rm p,AHD}(\tilde{\Omega}_+) + G_{\rm p,AHD}(\tilde{\Omega}_-)\right], \tag{A6}$$

where

$$\tilde{\Omega}_{\pm} = \frac{8 \pm \sqrt{13/3}}{5}\Omega \approx \{1.18\Omega, 2.02\Omega\}. \quad \text{(A7)}$$

We have tested the accuracy of the approximate integrator and found that the error was less than 1 per cent in the regime where $F_{\rm p}$, $G_{\rm p}$ have significant values, i.e. for $\Omega \lesssim \Omega_{\rm th} = \sqrt{3kT/I_3}$. More precisely, we checked that

$$\frac{|\Delta F_{\rm p}(\Omega)|}{F_{\rm p}(\Omega)} \times \min\left(1, \frac{F_{\rm p}(\Omega)}{F_{\rm p}(\Omega_{\rm th})}\right) < 0.01 \quad \text{(A8)}$$

for grain radii $a = 4, 5, 6$ Å, gas temperatures $T = 50, 500, 5000$ K and grain charge $Z = -1, 0, 1$, and similarly for $G_{\rm p}$.

This paper has been typeset from a TEX/LATEX file prepared by the author.